Cell Reports

Article

Protein nanoparticle vaccines induce potent neutralizing antibody responses against MERS-CoV

Graphical abstract

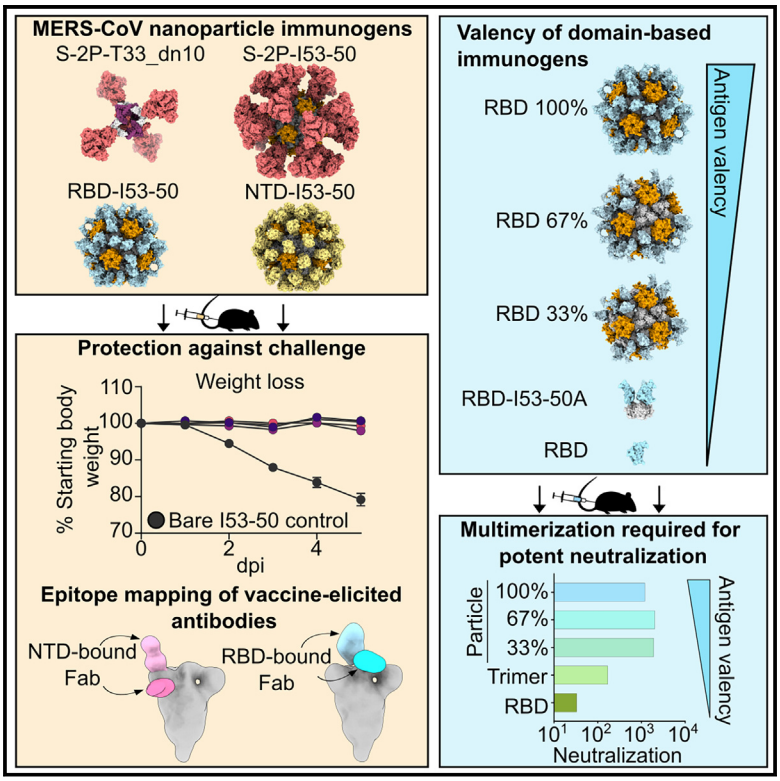

Highlights

- Design of protein nanoparticle immunogens displaying MERS-CoV spike-derived antigens
- Soluble MERS-CoV spike and nanoparticle immunogens are highly immunogenic in mice
- Polyclonal epitope mapping defines sites targeted by vaccine-elicited antibodies
- MERS-CoV immunogens protect mice against severe disease upon virus challenge

Authors

Cara W. Chao, Kaitlin R. Sprouse, Marcos C. Miranda, ..., Alexandra Schäfer, David Veesler, Neil P. King

Correspondence

neilking@uw.edu

In brief

Efficacious vaccines developed during the SARS-CoV-2 pandemic provide templates for other betacoronavirus vaccines. Chao et al. describe the development of protein nanoparticle immunogens displaying MERS-CoV antigens. The vaccines elicit neutralizing antibody responses and protection during viral challenge. This study extends a successful vaccine modality for sarbecoviruses to the merbecovirus subgenus.

Chao et al., 2024, Cell Reports *43*, 115036
December 24, 2024
https://doi.org/10.1016/j.celrep.2024.115036

CellPress

Cell Reports

CellPress
OPEN ACCESS

Article

Protein nanoparticle vaccines induce potent neutralizing antibody responses against MERS-CoV

Cara W. Chao,[1,2,3] Kaitlin R. Sprouse,[2] Marcos C. Miranda,[1,2,9] Nicholas J. Catanzaro,[4] Miranda L. Hubbard,[4] Amin Addetia,[2] Cameron Stewart,[2] Jack T. Brown,[2] Annie Dosey,[1,2] Adian Valdez,[1,2] Rashmi Ravichandran,[1,2] Grace G. Hendricks,[1,2] Maggie Ahlrichs,[1,2] Craig Dobbins,[1,2] Alexis Hand,[1,2,10] Jackson McGowan,[1,2] Boston Simmons,[1,2] Catherine Treichel,[1,2,11] Isabelle Willoughby,[1,2] Alexandra C. Walls,[2] Andrew T. McGuire,[2,6,7,8] Elizabeth M. Leaf,[1,2] Ralph S. Baric,[4] Alexandra Schäfer,[4] David Veesler,[2,5] and Neil P. King[1,2,12,*]

[1]Institute for Protein Design, University of Washington, Seattle, WA 98195, USA
[2]Department of Biochemistry, University of Washington, Seattle, WA 98195, USA
[3]Graduate Program in Molecular and Cellular Biology, University of Washington, Seattle, WA 98195, USA
[4]Department of Epidemiology, University of North Carolina at Chapel Hill, Chapel Hill, NC 27514, USA
[5]Howard Hughes Medical Institute, Seattle, WA 98195, USA
[6]Vaccine and Infectious Disease Division, Fred Hutchinson Cancer Research Center, Seattle WA 98109, USA
[7]Department of Global Health, University of Washington, Seattle, WA 98195, USA
[8]Department of Laboratory Medicine and Pathology, University of Washington, Seattle WA 98115, USA
[9]Present address: Washington University in St. Louis, St. Louis, MO, USA
[10]Present address: Mayo Clinic in Arizona, Phoenix, AZ, USA
[11]Present address: University of Bristol, Bristol, UK
[12]Lead contact
*Correspondence: neilking@uw.edu
https://doi.org/10.1016/j.celrep.2024.115036

SUMMARY

Middle East respiratory syndrome coronavirus (MERS-CoV) is a betacoronavirus that causes severe respiratory illness in humans. There are no licensed vaccines against MERS-CoV and only a few candidates in phase I clinical trials. Here, we develop MERS-CoV vaccines utilizing a computationally designed protein nanoparticle platform that has generated safe and immunogenic vaccines against various enveloped viruses, including a licensed vaccine for severe acute respiratory syndrome coronavirus 2 (SARS-CoV-2). Two-component nanoparticles displaying spike (S)-derived antigens induce neutralizing responses and protect mice against challenge with mouse-adapted MERS-CoV. Epitope mapping reveals the dominant responses elicited by immunogens displaying the prefusion-stabilized S-2P trimer, receptor binding domain (RBD), or N-terminal domain (NTD). An RBD nanoparticle elicits antibodies targeting multiple non-overlapping epitopes in the RBD. Our findings demonstrate the potential of two-component nanoparticle vaccine candidates for MERS-CoV and suggest that this platform technology could be broadly applicable to betacoronavirus vaccine development.

INTRODUCTION

The recent severe acute respiratory syndrome coronavirus 2 (SARS-CoV-2) pandemic has demonstrated the human and economic toll that can accompany the spillover and spread of a zoonotic disease in humans. Although the success of vaccine development efforts in response to the pandemic were a triumph of modern vaccinology, SARS-CoV-2 remains the only coronavirus for which licensed vaccines are available. To date, nine coronaviruses are known to infect humans, three of which (SARS-CoV, Middle East respiratory syndrome [MERS]-CoV, and SARS-CoV-2) have caused epidemics or pandemics in the last 20 years, and two of which (CCoV-HuPn-2018 and porcine deltacoronavirus) have been identified in humans in only the past 3 years, underscoring that more coronaviruses than previously appreciated pose zoonotic threats.[1–6] Developing vaccines for additional coronaviruses, both known and unknown, is therefore a public health priority.[7]

Among the known human-infecting coronaviruses, MERS-CoV stands out due to its high case fatality rate, estimated at 35%.[8,9] Since its discovery in 2012, MERS-CoV infections have been reported in 27 countries, mostly from contact with dromedary camels, although sporadic human-to-human transmission has also occurred.[10] Beyond its immediate value in the prevention of severe respiratory disease and death caused by MERS-CoV infection, a safe and effective MERS-CoV vaccine would provide a foundation for developing broadly protective vaccines that could prevent zoonotic spillover of known or unknown members of the merbecovirus subgenus. Three MERS-CoV vaccine candidates have entered clinical trials, although none has advanced to licensure.[11–13]

As the major surface antigen and the target of neutralizing antibodies, the spike (S) protein has been the focus of most MERS-CoV vaccine development efforts. S is a large trimeric class I viral fusion protein that is cleaved into two subunits, S_1 and S_2.[14] S_1 contains the N-terminal domain (NTD) and receptor binding

domain (RBD), which mediate virus attachment to host cells by binding sialosides and the proteinaceous receptor dipeptidyl peptidase 4 (DPP4), respectively.[15–19] S_2 comprises the fusion machinery that merges the virus and host membranes. Several studies have shown that the majority of serum neutralizing activity after infection or immunization, as well as the most potently neutralizing monoclonal antibodies, target the RBD and NTD,[20–27] although neutralizing and protective antibodies targeting S_2 have also been characterized.[28–36] Immunization with the MERS-CoV RBD, S_1, S_2, full-length S, and prefusion-stabilized S ectodomain have been evaluated in preclinical animal models and found to induce robust antibody responses and, in some cases, protection against challenge.[20,21,24,25,28,30,37–42] Nevertheless, vaccine design technologies and lessons from SARS-CoV-2 vaccine development efforts may allow the generation of vaccine candidates with improved safety, immunogenicity, and manufacturability.

A major lesson of the recent SARS-CoV-2 pandemic was that pre-existing platform technologies were essential for rapid vaccine development. For example, the prefusion-stabilizing 2P mutations that were identified using MERS-CoV as a prototype pathogen in 2017[40] enabled essentially immediate structure determination and vaccine design based on the SARS-CoV-2 spike.[42–44] The readiness of mRNA as a rapid response vaccine platform also proved critical.[45,46] Additional platform technologies were clinically de-risked during the pandemic, including computationally designed two-component protein nanoparticle vaccines.[47,48] Over the last several years, our groups and others have shown that these immunogens elicit potent neutralizing antibody responses against a number of viral pathogens by efficiently trafficking to lymph nodes and enhancing B cell activation.[39,49–60] In response to the SARS-CoV-2 pandemic, we developed a nanoparticle vaccine that displays 60 copies of the SARS-CoV-2 RBD on the icosahedral nanoparticle I53-50.[61] RBD-I53-50 induced robust neutralizing antibody responses in mice and nonhuman primates and was found to be safe and immunogenic in clinical trials, leading to its licensure in multiple jurisdictions under the name SKYCovione.[47,62–65] Collectively, these results suggest that two-component nanoparticles may be a robust and versatile vaccine platform.

Here, we generate two-component protein nanoparticle immunogens of diverse geometries displaying the MERS-CoV S-2P trimer, RBD, or NTD that elicit potent neutralizing antibody responses targeting antigenic sites in the S_1 subunit. Our findings identify several promising vaccine candidates for further development and establish two-component nanoparticles as a generalizable platform for betacoronavirus vaccine development.

RESULTS

Production and characterization of nanoparticle immunogens

Based on our successful previous application of two-component self-assembling nanoparticles to the development of sarbecovirus vaccines,[39,47,62,64,65] we set out to evaluate a series of nanoparticle immunogens for MERS-CoV. The prefusion-stabilized MERS S-2P trimer has been shown previously to elicit neutralizing antibodies in mice as a soluble trimer,[40] when displayed on nanoparticles,[39] or when delivered by mRNA.[42] To further explore the immunogenicity of this antigen, we displayed 4 or 20 copies of the S-2P trimer on two distinct nanoparticles, T33_dn10 and I53-50. T33_dn10 is composed of four copies each of two different designed trimeric proteins that assemble into a 24-subunit nanoparticle with tetrahedral symmetry,[66] while I53-50 is constructed from 12 pentamers and 20 trimers that form a 120-subunit complex with icosahedral symmetry.[61] In each case, the S-2P ectodomain trimer with a C-terminal foldon was genetically fused to a trimeric component with externally oriented N termini (Figure 1A; Table S1). Given the success of our RBD-I53-50 nanoparticle vaccine against SARS-CoV-2[47,62] and the key role of the NTD in the attachment of MERS-CoV to cells,[18,19] we also evaluated I53-50-based nanoparticle immunogens displaying the MERS-CoV RBD or NTD. We genetically fused these domain-based antigens to the N terminus of the I53-50A trimer to enable display of 60 copies on the I53-50 nanoparticle in a manner analogous to our previously described SARS-CoV-2 RBD nanoparticle vaccine.[62]

We secreted these glycoprotein antigen-bearing components from transfected Expi293F cells and purified them from clarified supernatants using immobilized metal affinity chromatography. We also expressed and purified the soluble MERS-CoV S-2P trimer as a fusion to the foldon trimerization domain for use as a benchmark. Size exclusion chromatography (SEC) of the S-2P-T33_dn10A and S-2P-I53-50A trimers showed that these components eluted at the same volume as the S-2P foldon trimer, while the RBD- and NTD-I53-50A components eluted later, as expected due to their smaller size (Figures 1B and S1A). After mixing each antigen-bearing component with the appropriate second component (i.e., trimeric T33_dn10A or pentameric I53-50B), a shift to an earlier SEC elution volume was observed, suggesting nanoparticle assembly. Small amounts of residual unassembled components were observed in the S-2P- and RBD-I53-50 assembly reactions, as expected given that each contained a slight excess of the trimeric component (STAR Methods). Analysis of the SEC-purified nanoparticles by SDS-PAGE confirmed that each preparation contained both of the expected protein components, and dynamic light scattering (DLS) indicated monodisperse nanoparticles with the expected hydrodynamic diameters (Figures S1B and S1C). Negative stain electron microscopy (nsEM) supported the SEC and DLS data, revealing fields of monodisperse nanoparticles of the expected sizes and shapes. S-2P-T33_dn10 clearly displayed four copies of the S-2P trimer, although these were flexibly linked to the underlying nanoparticle core; we obtained separate classes during 2D averaging corresponding to the tetrahedral nanoparticle and the displayed prefusion S trimer (Figure 1C). nsEM of S-2P-I53-50 revealed spherical assemblies densely decorated with spikes that resembled micrographs previously obtained for sarbecovirus S-I53-50 immunogens.[67–69] RBD- and NTD-I53-50 also formed well-defined nanoparticles with additional densities on the nanoparticle surface, although these were less clearly defined than displayed S-2P due to the smaller size of the RBD and NTD antigens. Having confirmed expression of the antigen-bearing components and assembly of the nanoparticle immunogens, we next sought to evaluate retention of antigenicity

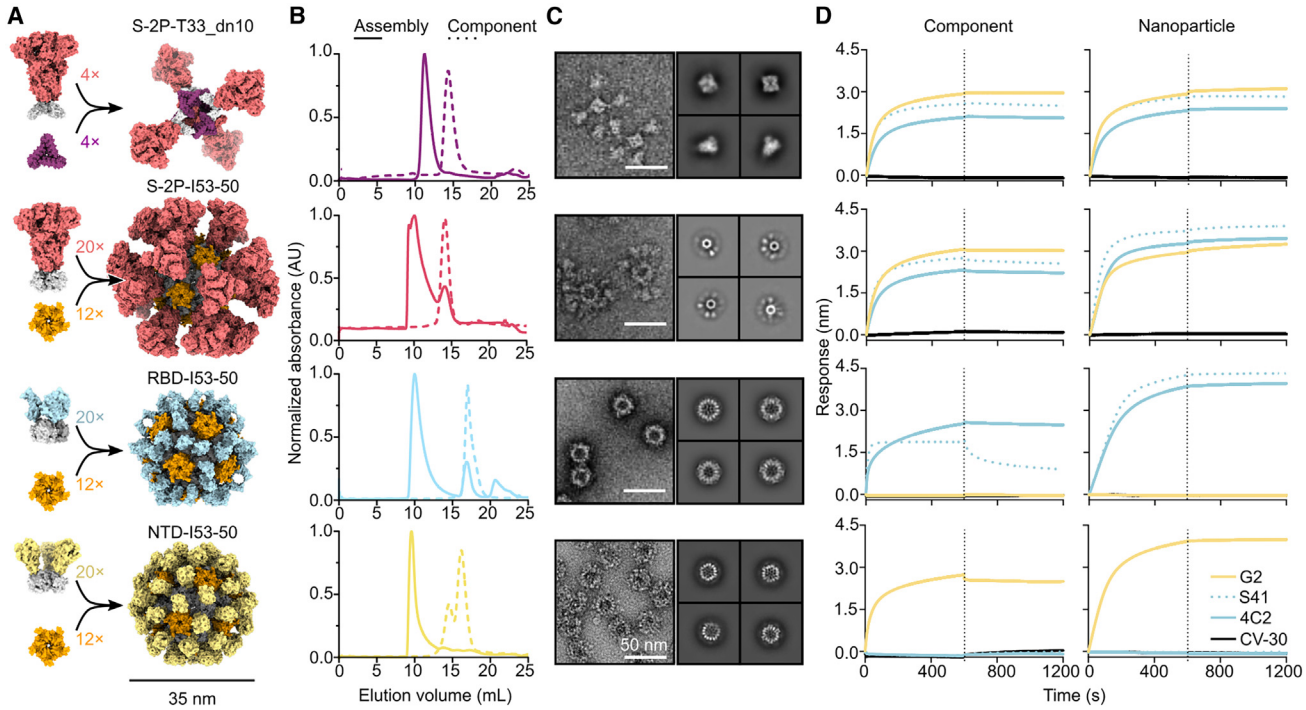

Figure 1. Production and characterization of nanoparticle immunogens

(A) Schematics of MERS-CoV nanoparticle immunogen assembly.

(B) Size exclusion chromatograms of MERS-CoV nanoparticle components (dotted lines) and assembled nanoparticles (solid lines) on a Superose 6 10/300 GL.

(C) Raw micrographs (left) and 2D class averages (right) of negatively stained SEC-purified nanoparticles. For S-2P-T33_dn10, class averages of the nanoparticle core and displayed S-2P trimer are shown at the top and bottom, respectively. Scale bar, 50 nm.

(D) Binding of (left) antigen-bearing components prior to assembly and (right) SEC-purified nanoparticle immunogens to mAbs G2 (NTD specific), S41 (RBD specific), 4C2 (RBD specific), and CV-30 (SARS-CoV-2 S RBD specific, negative control).

using biolayer interferometry and a panel of conformation-specific monoclonal antibodies (mAbs) (Figure 1D). As expected, the two RBD-specific antibodies S41[70] and 4C2[24] bound to all antigen-bearing components and nanoparticles except for NTD-I53-50A and NTD-I53-50. Conversely, the NTD-directed antibody G2[20,27] bound to all constructs except RBD-I53-50A and RBD-I53-50. Dissociation was unambiguously observed only for the RBD-I53-50A–S41 complex; as expected, the highly avid interactions between the corresponding RBD-I53-50 nanoparticle and the S41 mAb prevented dissociation. Our negative control antibody CV-30, a SARS-CoV-2 S RBD-directed neutralizing antibody isolated from a convalescent patient,[71] did not bind to any of our MERS constructs. Together, these data demonstrate the production of a series of well-defined and antigenically intact nanoparticle immunogens for MERS-CoV displaying the prefusion-stabilized S-2P trimer, RBD, or NTD.

Antibody responses elicited by MERS-CoV nanoparticle immunogens in mice

We evaluated the immunogenicity of our MERS-CoV nanoparticles by measuring antigen-specific and neutralizing antibody titers in serum after immunizing groups of 10 BALB/c mice twice with AddaVax-adjuvanted immunogens 4 weeks apart (Figure 2A). Two weeks post prime, the highest levels of S-2P-specific antibodies were observed in the sera of animals that received RBD-I53-50 (geometric mean titer [GMT] half maximal effective concentration of 5.6×10^3), followed by S-2P-I53-50 (1.6×10^3); all other groups had GMTs $<10^3$ (Figures 2B and S2A). Two weeks post boost, all groups but the bare I53-50 nanoparticle control showed high antibody titers, ranging from $3.2–8.4 \times 10^4$, that waned slightly by week 8 ($7.0 \times 10^3–1.9 \times 10^4$). S-2P, S-2P-T33_dn10, and, to a lesser extent, S-2P-I53-50 elicited serum antibodies that bound to SARS-CoV and SARS-CoV-2 HexaPro-foldon trimers,[72] but we did not observe similar cross-reactivity from the nanoparticles displaying the domain-based antigens (Figures S2B and S2C). Upon further investigation, these sera bound similarly to an influenza hemagglutinin-foldon trimer but not to an OC43 S-2P trimer fused to the GCN4 tetramerization domain, implicating anti-foldon antibodies, which we subsequently confirmed by nsEM polyclonal epitope mapping (ns-EMPEM; Figure S2D).[73,74] Antibody responses against the T33_dn10 and I53-50 nanoparticle scaffolds were also observed in sera from the expected groups (Figures S2E and S2F).

Serum neutralizing activity against a panel of vesicular stomatitis virus (VSV) pseudotypes bearing closely related MERS-CoV spikes (EMC, London, Kenya, and South Korea; the latter three have 99% amino acid identity to the vaccine strain; Table S1) largely mirrored the binding antibody titers. Specifically, RBD-I53-50 was the only immunogen that elicited appreciable neutralizing activity post prime (EMC strain GMT 0.7×10^2 and Kenya

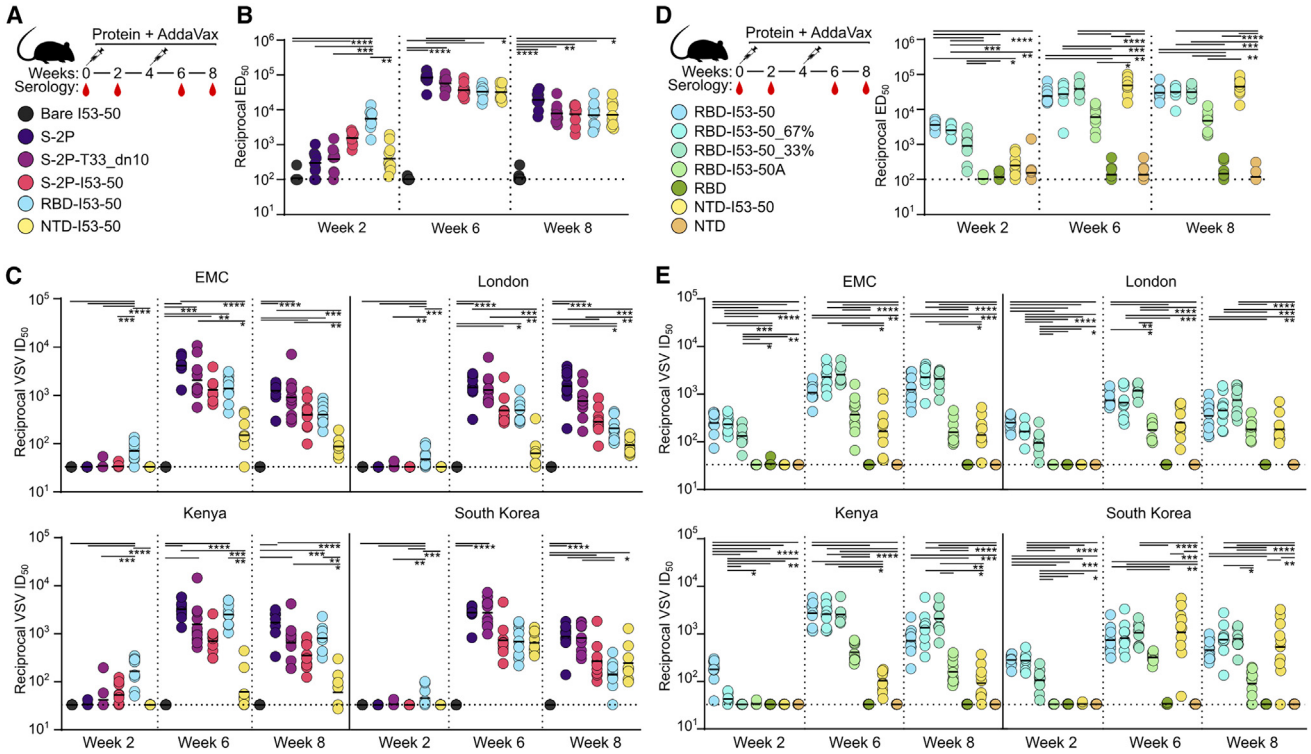

Figure 2. Antibody responses elicited by MERS-CoV nanoparticle immunogens in mice

(A) Study design and groups. Groups of 10 BALB/c mice were immunized at weeks 0 and 4, and serum was obtained at weeks 0, 2, 6, and 8.

(B) Serum antibody binding titers against vaccine-matched (EMC) MERS-CoV S-2P, measured by ELISA.

(C) Vaccine-elicited neutralizing activity against VSV pseudotyped with closely related MERS-CoV EMC, London variant, Kenya variant, or South Korea variant spikes. The mouse immunization study was performed twice, and representative data from one study are shown.

(D) Left: domain-based antigen study design and groups. Groups of 10 BALB/c mice were immunized at weeks 0 and 4 and bled at weeks 0, 2, 6, and 8. Right: serum antibody binding titers against vaccine-matched (EMC) MERS-CoV S-2P, measured by ELISA.

(E) Vaccine-elicited neutralizing activity against VSV pseudotyped with closely related MERS-CoV EMC, London variant, Kenya variant, or South Korea variant S. In (B). (C), (D), and (E), all groups were compared with Kruskal-Wallis test followed by Dunn's multiple-comparisons test. $^{****}p < 0.0001$, $^{***}p < 0.001$, $^{**}p < 0.01$, $^{*}p < 0.1$. Only significant differences are shown. See supplemental information for all statistical comparisons.

strain GMT 1.6 × 10^2), while potent neutralization was observed post boost for all groups at week 6 with slight subsequent waning by week 8 (Figures 2C and S3). Slightly more separation between the groups was observed in the post-boost neutralization data than in the antigen-specific antibody titers. Specifically, the soluble S-2P trimer and S-2P-T33_dn10 generally induced the highest titers, although these were not significantly different from those induced by S-2P-I53-50. Nevertheless, given that several previous studies have found that immunogenicity tends to increase with increasing antigen valency[50,75,76] and that we had previously observed that a SARS-CoV-2 RBD-I53-50 nanoparticle elicited more potent neutralizing activity than the corresponding S-2P trimer,[62] we investigated potential causes for the lower-than-expected immunogenicity of S-2P-I53-50 relative to the S-2P trimer and S-2P-T33_dn10. First, we compared the thermal stabilities of the SARS-CoV-2 and MERS-CoV S-2P trimers, as previous studies have demonstrated that more stable antigens give rise to enhanced immunogenicity.[72,77–79] However, we did not find substantial differences in stability (Figure S4A), suggesting that other mechanisms likely account for the improved performance of the MERS-CoV S-2P trimer relative to RBD-I53-50 compared to the analogous SARS-CoV-2 immunogens. When analyzing the S-2P-I53-50 nanoparticle, we noticed increasing amounts of unassembled components in electron micrographs prepared from the later fractions of the broad SEC peak obtained after *in vitro* assembly (Figure S4B). We also found that S-2P-I53-50 aggregated upon heating, whereas the S-2P-T33_dn10 nanoparticles did not aggregate at temperatures up to 95°C (Figure S4C). These data indicated heterogeneity and instability in the S-2P-I53-50 nanoparticles, which is atypical for I53-50-based immunogens. The levels of neutralization after boosting with the RBD-I53-50 nanoparticle often trended slightly lower than the S-2P-based immunogens, although this only reached significance in a couple of cases (i.e., against the London and South Korea variants). By contrast, sera from mice that received the NTD-I53-50 nanoparticle consistently had significantly lower neutralizing activity than the other immunogens with the exception of neutralization of the South Korea variant, which contains an H91Y mutation in the sialic acid binding site of the NTD that may sensitize it to neutralization.[18,19]

Previous work from our group and others has shown that displaying domain-based antigens on nanoparticles significantly

improves their immunogenicity.[51,62,80–85] To evaluate the effect of multimerization on the immunogenicity of the MERS-CoV RBD and NTD, we immunized groups of 10 BALB/c mice twice with 1 μg of RBD-I53-50, the trimeric RBD-I53-50A component alone, NTD-I53-50, monomeric RBD, or monomeric NTD, each formulated with AddaVax (Figure 2D). We also included groups of mice that received partial-valency RBD-I53-50 nanoparticles in which only 67% or 33% of the trimeric components comprised the RBD as a genetic fusion. Similar to our first study, RBD-I53-50 at 100% valency elicited high levels of S-2P-directed antibody responses after the primary immunization (GMT 3.5×10^3), while NTD-I53-50 yielded lower titers (GMT $< 10^3$) (Figures 2D and S5). Among the three RBD nanoparticles tested, there appeared to be a slight decrease in immunogenicity with decreasing RBD valency, although the differences between groups were not statistically significant. By contrast, the trimeric RBD-I53-50A and RBD and NTD monomer groups all had minimal responses (GMT $< 10^3$). Two weeks post boost, all nanoparticle groups displayed comparably high antibody titers (2.4×10^4–4.8×10^4), the RBD-I53-50A group was somewhat lower (6.0×10^3), and the monomeric RBD and NTD still failed to induce robust antibody responses. These antigen-specific antibody titers were essentially unchanged in sera obtained at week 8.

Vaccine-elicited neutralizing activity largely mirrored these observations except that the NTD-I53-50 nanoparticle generally elicited significantly lower levels of neutralization than RBD-I53-50 (Figures 2E and S6). Notably, all three of the RBD-I53-50 nanoparticles induced detectable neutralizing activity after the primary immunization, while the RBD-I53-50A trimer and the RBD and NTD monomers failed to do so. No change was observed after a second immunization with the monomeric RBD and NTD, while sera from the RBD-I53-50A group yielded detectable neutralization at week 6 and 8 that was lower than that of the RBD-I53-50 nanoparticle groups although not always significantly so. These data, in contrast to the S-2P-based immunogens, clearly demonstrate that multimerization significantly enhances the immunogenicity of the domain-based RBD and NTD antigens.

Epitope mapping of vaccine-elicited antibodies

We used serum competition assays to map the specificity of the antibody responses elicited by the S-2P trimer and nanoparticle immunogens during the immunogenicity study depicted in Figure 2A. We measured the week 8 serum dilutions required to compete with hDPP4 and G2 binding to examine receptor-blocking and NTD-directed responses, respectively (Figures 3A and S7A–S7C). We observed comparable hDPP4 competition across the S-2P, S-2P-T33_dn10, S-2P-I53-50, and RBD-I53-50 groups, suggesting that all of these vaccines induced similar levels of receptor-blocking antibodies (Figure S7D). The bare I53-50 nanoparticle control group did not elicit detectable hDPP4- or G2-competing antibodies as expected. We observed more variation among immunogens in the competition of our polyclonal sera with G2 (Figure S7E). Although none of the sera completely blocked G2 binding under the conditions tested, they could be stratified into three groups. Sera from mice that received NTD-I53-50 and S-2P-T33_dn10 most potently competed with G2 binding, followed by the S-2P trimer and S-2P-I53-50, followed by the RBD-I53-50 nanoparticle. The competition from RBD-I53-50-induced antibodies, albeit weak, was consistent across the sera from all mice. We interpret these data to indicate that some RBD-directed antibodies sterically compete with the binding of NTD-directed antibodies, a phenomenon that is similar to blockade of DPP4 binding by some NTD-directed antibodies.[25,27]

We next visualized the dominant serum antibody specificities elicited by the S-2P trimer and the three I53-50 nanoparticle immunogens using ns-EMPEM. To do this, we first generated a low-resolution reconstruction of the MERS-CoV S-2P trimer, which was consistent with structures obtained in previous reports (Figure 3B).[19,40,74] We then pooled and processed mouse sera from week 10 to generate polyclonal antibody fragment (Fab) complexes with MERS-CoV S-2P and mapped the densities obtained from ns-EMPEM onto the S-2P trimer reconstruction. In sera from mice immunized with soluble S-2P, we observed two slightly distinct classes of NTD-directed Fabs that bind the antigenic site targeted by G2 and many NTD-directed neutralizing antibodies against SARS-CoV-2 (Figure 3C).[27,86–88] We did not detect RBD-directed Fab classes using these sera, possibly due to spike triggering and unfolding.[89,90] In sera from mice immunized with S-2P-T33_dn10, we observed three classes of Fabs, two of which appeared to be NTD directed and resembled those seen in the S-2P group, while the third could be visualized in 2D class averages but could not be resolved during 3D reconstruction (Figure 3D). We also only observed NTD-directed Fab classes in the sera of mice that received S-2P-I53-50 (Figure 3E). One of the two dominant classes targeted the same antigenic site at the apex of the NTD, while the second class bound the side of the NTD with an almost perpendicular angle of approach and was similar to the unresolved density observed in sera from mice immunized with S-2P-T33_dn10. Interestingly, these two classes recapitulate the specificities of cross-reactive antibodies against MERS-CoV S-2P identified in a recent study after immunization with a two-component nanoparticle immunogen displaying the SARS-CoV S-2P trimer.[39]

As expected, the domain-based NTD- and RBD-I53-50 nanoparticle immunogens elicited antibodies that bind each respective domain. All of the Fab-antigen complexes observed in the anti-NTD-I53-50 sera target the antigenic site at the apex of the NTD; we did not see 2D classes showing Fabs bound to the side of the NTD as we did for S-2P-T33_dn10 and S-2P-I53-50 (Figure 3F). By contrast, in sera from mice immunized with RBD-I53-50, we observed a number of distinct classes of antibodies targeting various epitopes, including those bound to both "up" and "down" RBDs (Figure 3G). Strikingly, several 2D class averages clearly showed multiple Fabs bound simultaneously to the same RBD, indicating that they bind non-overlapping epitopes.

Our inability to resolve RBD-directed densities from the soluble S-2P and S-2P-I53-50 groups was surprising given the apparent immunodominance of the RBD in MERS-CoV and other coronaviruses.[91–94] Furthermore, our hDPP4 competition data clearly indicate the presence of high levels of RBD-directed antibodies in these sera (Figure 3A). We note that we had to optimize our experimental conditions to prevent destabilization of the spike protein[95] by shortening the polyclonal Fab-antigen

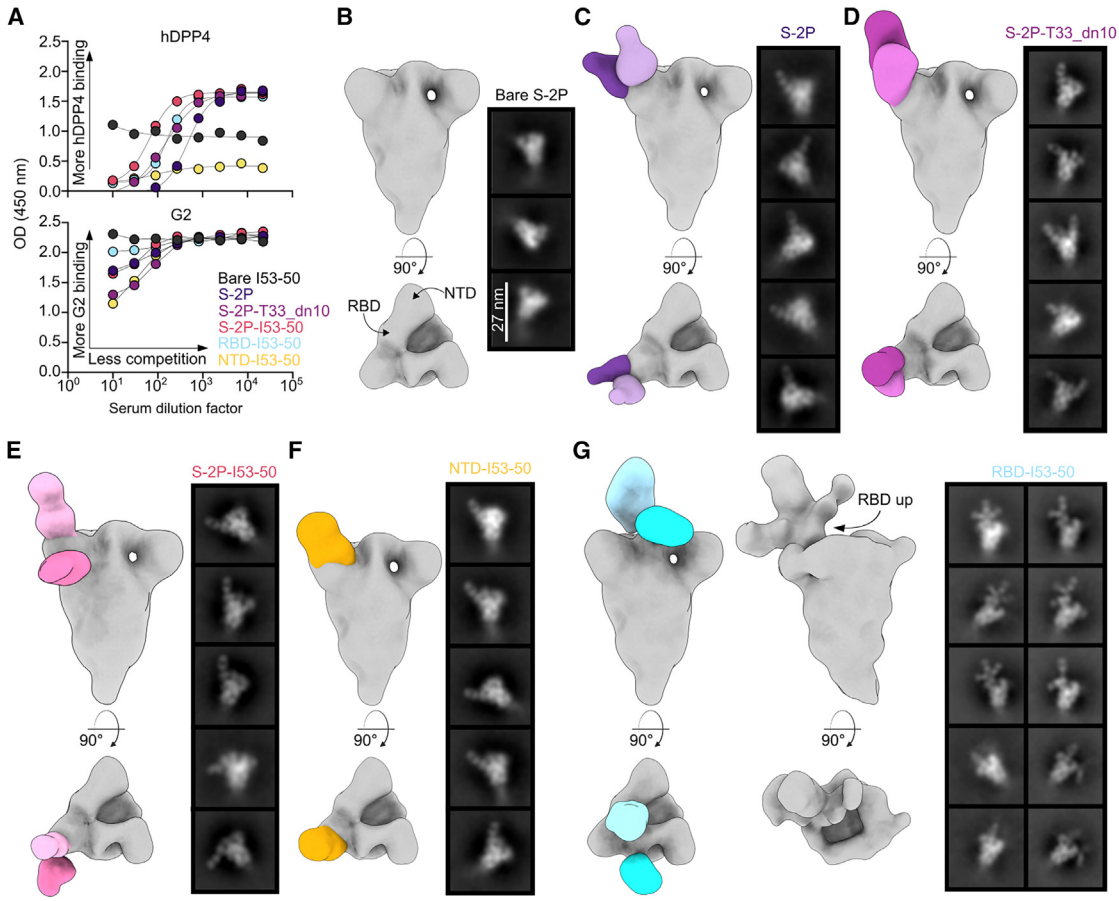

Figure 3. Epitope mapping of vaccine-elicited antibodies

(A) Serum competition of study groups with hDPP4 (top) and G2 (bottom) against MERS-CoV S-2P.

(B) Composite 3D model of MERS S-2P with no bound Fabs and representative 2D class averages. Scale bar, 27 nm.

(C–G) Composite 3D models and representative 2D class averages of ns-EMPEM analysis depicting Fab-bound MERS S-2P spikes from week 8 sera from mice immunized with S-2P (C), S-2P-T33_dn10 (D), S-2P-I53-50 (E), NTD-I53-50 (F), and RBD-I53-50 (G). In (G), a composite 3D model is shown to visualize Fabs bound to a "three-down" MERS-CoV S, while a separate 3D reconstruction is shown to visualize Fabs bound to an RBD in the "up" conformation.

incubation time and using a lower molar ratio of polyclonal Fabs to antigen (STAR Methods). It is likely that these conditions prevented us from observing all Fab classes prevalent in the sera. As a result, we only provide qualitative interpretations of our ns-EMPEM data. Nevertheless, taken together, our epitope mapping data suggest that the RBD and NTD of the MERS-CoV spike are immunodominant during vaccination, as observed in many studies of antibody responses to SARS-CoV-2[92,96–99] and a limited number of studies of other betacoronaviruses.[74,93,97,98] Our results further suggest that a single antigenic site is immunodominant in the NTD, whereas several antigenic sites in the RBD are highly immunogenic.

Protection against challenge with mouse-adapted MERS-CoV

Finally, we evaluated the protection afforded by each immunogen in a mouse immunogenicity and challenge study. We immunized 288/330$^{+/+}$ mice that express a chimeric DPP4 receptor in the C57BL/6J genetic background with two doses of our S-2P or RBD-based immunogens and subsequently challenged them at study week 15 with 1 × 10^5 plaque-forming units of mouse-adapted MERS-CoV (maM35c4) (Figure 4A). This model has been shown previously to recapitulate many aspects of the acute respiratory distress syndrome that humans experience upon MERS-CoV infection.[100,101] The levels of S-2P-specific antibodies in sera collected 2 weeks post prime and post boost were generally similar to those observed in our earlier study in BALB/c mice, except that the post-prime titers were slightly higher for the S-2P-based immunogens in this study (Figures 4B and S8A). Similar results were obtained in pseudovirus neutralization assays; the data mirrored our earlier BALB/c immunogenicity study except that the S-2P-displaying nanoparticles induced detectable neutralizing activity at week 2 in addition to the RBD-I53-50 nanoparticle (Figures 4C and S8B). Overall, the trends in antigen-specific and neutralizing antibody titers between the 288/330$^{+/+}$ and BALB/c mice were comparable, showing slightly higher responses from the nanoparticle groups after priming and similar responses after boosting.

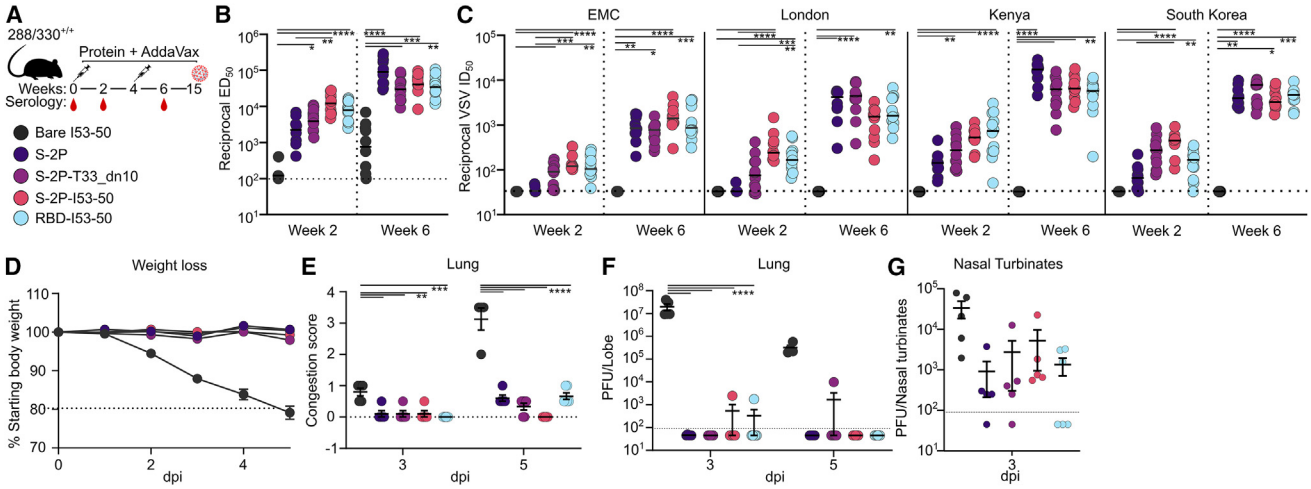

Figure 4. Protection against challenge with mouse-adapted MERS-CoV

(A) Challenge study design and groups. Groups of 288/330$^{+/+}$ mice were immunized at weeks 0 and 4; serum was obtained at weeks 0, 2, and 6; and the mice were challenged at week 15.

(B) Serum antibody binding titers against vaccine-matched (EMC) MERS-CoV S-2P, measured by ELISA.

(C) Vaccine-elicited neutralizing activity against VSV pseudotyped with closely related MERS-CoV EMC, London variant, Kenya variant, or South Korea variant spikes. Groups were compared using Kruskal-Wallis test followed by Dunn's multiple-comparisons test. ****$p < 0.0001$, ***$p < 0.001$, **$p < 0.01$, *$p < 0.1$.

(D) Changes in body weight after maM35c4 challenge. Data are represented as mean ± SEM.

(E) Lung congestion score. Data were analyzed with two-way ANOVA or mixed model followed by Sidak's multiple comparison. ****$p < 0.0001$, ***$p < 0.001$, **$p < 0.01$. Data are represented as mean ± SEM.

(F) Viral titers in the lungs of challenged mice from 3 days post infection (dpi): $n = 5$ for bare I53-50, S-2P, S-2P-T33_dn10, and S-2P-I53-50; $n = 6$ for RBD-I53-50. 5 dpi: $n = 4$ for bare I53-50; $n = 5$ for S-2P and S-2P-I53-50; $n = 6$ for S-2P-T33_dn10 and RBD-I53-50. Data were analyzed with two-way ANOVA or mixed model followed by Dunnett's multiple-comparison test. ****$p < 0.0001$. Data are represented as mean ± SEM.

(G) Viral titers in nasal turbinates of challenged mice. $n = 5$ for bare I53-50, S-2P, S-2P-T33_dn10, and S-2P-I53-50; $n = 6$ for RBD-I53-50. Data were analyzed with one-way ANOVA with Geisser-Greenhouse correction followed by Dunnett's multiple-comparison test.

In (B), (C), (E), (F), and (G), only significant differences are shown; see supplemental information for all statistical comparisons. Data are represented as mean ± SEM.

maM35c4 challenge at week 15 allowed us to evaluate the efficacy of our immunogens against the development of severe disease. All 11 control mice immunized with two doses of bare I53-50 lost 20% of their starting weight by day 5 post infection and had to be euthanized (Figure 4D). By contrast, all mice given two doses of MERS-CoV immunogens were protected from severe disease, showing no appreciable weight loss after infection. Furthermore, the mice receiving MERS immunogens displayed undetectable to mild lung damage 3 and 5 days post infection, while those receiving the bare I53-50 control immunogen showed considerable damage on day 5 (Figure 4E). While viral titers in the lungs were below the limit of detection in nearly all mice immunized with antigen-bearing immunogens throughout the duration of the experiment, viral titers in nasal turbinates were reduced ≥1–2 logs relative to those in the bare I53-50 control group 3 days post infection (Figures 4F and 4G). Together, these data show that immunization with prefusion-stabilized S-2P and a series of two-component nanoparticle immunogens elicited potent neutralizing antibody responses and protected 288/330$^{+/+}$ mice from developing severe disease when challenged with a lethal dose of maM35c4.

DISCUSSION

Here, we demonstrated that two-component nanoparticle vaccines elicit potent neutralizing activity and protective responses against a merbecovirus. The successful application of two-component nanoparticle vaccines to a second subgenus of betacoronaviruses suggests that their utility may extend even further across the Coronaviridae. Although several other protein nanoparticle technologies were evaluated as SARS-CoV-2 vaccines,[102–109] and some have begun to be applied to other betacoronaviruses,[110–112] to our knowledge, NVX-CoV2373 from NovaVax and the RBD-I53-50 nanoparticle vaccine SKYCovione are the only two that have obtained regulatory approval. Two-component protein nanoparticle vaccine candidates for RSV and RSV/HMPV have also been found to be safe and immunogenic in clinical trials (ClinicalTrials.gov: NCT05664334 and NCT05903183),[50] and a two-component mosaic nanoparticle vaccine for influenza virus is currently in phase I clinical trials (ClinicalTrials.gov: NCT04896086 and NCT05968989).[56] These precedents combine with the data presented here to establish two-component protein nanoparticles as a platform for pandemic preparedness vaccine development.

The SARS-CoV-2 pandemic led to a deep understanding of the mechanisms of antibody-mediated protection against a betacoronavirus. For SARS-CoV-2, although effector functions from non-neutralizing antibodies can also protect,[32,113–117] the most potently neutralizing antibodies target the RBD and a single immunodominant antigenic site in the NTD.[86,88,92,118,119] Our data extend those observations to merbecoviruses. The

immunogens we tested can be separated into three categories based on the antigen they comprise: the prefusion-stabilized S-2P trimer, the RBD, or the NTD. We found that all of the vaccine candidates tested, including those based on the S-2P trimer or nanoparticles displaying domain-based antigens, elicited robust neutralizing activity. The RBD-I53-50 nanoparticle elicited the most potent antibody responses after a single immunization, mirroring results we obtained previously for SARS-CoV-2.[62] However, unlike that study, the MERS-CoV S-2P-based immunogens tended to induce higher neutralizing activity post boost, though most of the differences were not statistically significant. Of the three antigens, nanoparticles displaying the NTD elicited the lowest neutralizing activity. Although the NTD has been less explored as a vaccine antigen, a recent report highlighted that most of the MERS-CoV neutralizing activity in the sera of infected humans targets the RBD and NTD,[94] and our results obtained with NTD-I53-50 clearly establish the neutralizing activity of vaccine-elicited antibodies against the NTD. These antibodies, like several previously described mAbs,[20,21,25,120,121] appear to primarily target a dominant antigenic site near the α-2,3-linked sialoside binding site.[19,27] The role of sialoside binding in MERS-CoV attachment to host cells suggests a potential mechanism for neutralization by NTD-directed antibodies beyond sterically blocking DPP4 engagement.[18] Nevertheless, given the lower neutralizing activity elicited by NTD-I53-50, the rapid evolution of the SARS-CoV-2 NTD during the pandemic,[88,122–124] and the high sequence diversity in merbecovirus NTDs, it is not clear that an NTD-based immunogen would be preferred for further development.

Comparing a series of MERS-CoV nanoparticle immunogens to corresponding soluble antigens led to several interesting findings. First, multivalent display of the prefusion S-2P trimer did not enhance immunogenicity beyond that of the soluble S-2P trimer. It must be noted that the immunogenicity of the S-2P-I53-50 nanoparticles may be compromised by their heterogeneity and instability. Given that we have shown previously that incomplete assembly can result in I53-50 nanoparticles with reduced physical stability,[125] we suspect that the prefusion spike trimer is large enough to hinder display at full valency on I53-50 and that some fraction of the preparations consisted of incomplete assemblies. If such incomplete assemblies also have compromised stability *in vivo*, then this may reduce their immunogenicity,[126] a hypothesis that can be tested in future studies. However, the S-2P-T33_dn10 nanoparticles were highly monodisperse and showed no evidence of instability, yet they were also not more immunogenic than the soluble S-2P trimer. Several previous studies that compared nanoparticles displaying prefusion-stabilized spike trimers from SARS-CoV, SARS-CoV-2, and MERS-CoV to their soluble counterparts made similar observations.[39,64,69,127] Alongside these studies, our results suggest that large, glycosylated antigens like prefusion spike trimers do not significantly benefit from nanoparticle display. Previous work has shown that glycosylated nanoparticle immunogens traffic more efficiently to lymph nodes and B cell follicles *in vivo* compared to non-glycosylated or soluble antigens, increasing their immunogenicity.[59,60,128] However, the large size of the prefusion S trimer and its extensive glycosylation may intrinsically confer this benefit and reduce the enhancement typically afforded by multimerization.

By contrast, we found that multivalent display of the RBD and NTD—both domain-based antigens—significantly improved their immunogenicity. Immunization with monomeric RBD or NTD failed to elicit neutralizing activity and barely resulted in detectable antigen-specific antibody in serum. While a trimerized version of the RBD performed better than the monomer, particularly after boosting, it was still substantially less immunogenic than the RBD-I53-50 nanoparticle. Together with the data on our spike-based immunogens, these results suggest that enhancing immunogenicity via nanoparticle display may be most effective for smaller antigens. Consistent with this, I53-50 nanoparticles displaying the RBD at different densities did not elicit significantly different levels of antigen-specific or neutralizing antibodies. This result may indicate that nanoparticle display enhances the immunogenicity of the RBD mainly by increasing its size and, therefore, presumably its trafficking *in vivo*, although we did not directly test that hypothesis here. Overall, our comparisons between particulate and soluble antigens simultaneously provide guidance on how to best apply nanoparticle display in vaccine design and raise interesting mechanistic questions that can be addressed in future studies.

In summary, we found that the prefusion-stabilized MERS-CoV S and several two-component nanoparticle immunogens induce robust and protective immune responses against MERS-CoV in vaccinated mice. The high performance of the S-2P spike and the RBD-I53-50 nanoparticle, and the use of the same platform as the licensed SARS-CoV-2 vaccine SKYCovione by the latter, motivate further development of these vaccine candidates. More generally, our data highlight two-component protein nanoparticle immunogens as a platform technology that may be broadly useful for designing vaccines against betacoronaviruses and other virus families.

Limitations of the study

One limitation of our study is that we were unable to resolve all vaccine-elicited antibody specificities by ns-EMPEM. This was highlighted by our inability to visualize RBD-bound Fabs in the groups administered immunogens based on the S-2P spike despite our observation of hDPP4-competing antibodies by ELISA. We suggest that this was due to polyclonal antibodies binding to multiple epitopes in the spike and triggering its disassembly, a phenomenon that has been observed for other class I viral fusion proteins.[129–131] Another limitation is that we did not evaluate the protective capacity of the NTD-I53-50 nanoparticle immunogen, leaving this as an open question for future studies. In addition, the challenge studies we did perform were limited to a mouse model. Although this model has been shown to reflect the acute respiratory distress syndrome observed in MERS-CoV-infected humans,[100,101] its capacity to predict vaccine performance in higher mammals is currently unknown. Finally, additional studies will be required to measure the breadth of antibody responses elicited by these MERS-CoV immunogens against other merbecoviruses. We note that the phylogenetic diversity of known merbecoviruses is growing, which may increase the number of vaccine

antigens required to develop broadly protective merbecovirus vaccines.[132–134]

RESOURCE AVAILABILITY

Lead contact

Requests for further information, resources, and reagents should be directed to and will be fulfilled by the lead contact, Neil King (neilking@uw.edu).

Materials availability

All unique and stable reagents generated in this study are available from the lead contact under a materials transfer agreement.

Data and code availability

- Structural data generated from this study were deposited in public data repositories, and the accession numbers are listed in the key resources table.
- This paper does not report original code.
- Any additional information required to reanalyze the data reported in this paper is available from the lead contact upon reasonable request.

ACKNOWLEDGMENTS

This study was supported by the National Institute of Allergy and Infectious Diseases (P01AI167966 to R.S.B., D.V., and N.P.K. and 75N93022C00036to D.V.), an Investigators in the Pathogenesis of Infectious Disease Award from the Burroughs Wellcome Fund (to D.V.), the National Science Foundation Graduate Research Fellowships Program Award (DGE-2140004 to C.W.C.), the University of Washington Arnold and Mabel Beckman cryoEM center and National Institutes of Health grant S10OD032290 (to D.V.), and the Audacious Project at the Institute for Protein Design (to N.P.K.). D.V. is an Investigator of the Howard Hughes Medical Institute and the Hans Neurath Endowed Chair in Biochemistry at the University of Washington. The authors thank Sebastian Ols, Cyrus Haas, Marti Tooley, Kenneth Carr, and Andrew Borst for helpful discussions.

AUTHOR CONTRIBUTIONS

C.W.C., M.C.M., A.C.W., D.V., and N.P.K. designed the study. C.W.C., M.C.M., and A.C.W. designed and characterized immunogens. C.W.C. and K.R.S. performed *in vitro* experiments, and N.J.C. performed challenge experiments. C.W.C., M.C.M., A.A., C.S., J.T.B., A.D., A.V., R.R., and G.G.H. produced proteins and provided reagents. C.T., I.W., E.M.L., M.L.H., J.M., and B.S. conducted and performed animal immunizations. M.A., C.D., and A.H. provided and maintained cells. C.W.C. and K.R.S. analyzed the data. A.T.M., A.S., and R.S.B. provided oversight of immunization and challenge studies. C.W.C., N.P.K., D.V., K.R.S., E.M.L., and A.S. wrote the manuscript with input from all authors.

DECLARATION OF INTERESTS

M.C.M., G.G.H., A.C.W., N.P.K., and D.V. are named as inventors on patent applications filed by the University of Washington related to coronavirus vaccines. The King lab has received unrelated sponsored research agreements from Pfizer and GSK.

STAR★METHODS

Detailed methods are provided in the online version of this paper and include the following:

- KEY RESOURCES TABLE
- EXPERIMENTAL MODEL AND STUDY PARTICIPANT DETAILS
  - Cell lines
  - Mice
- METHOD DETAILS
  - Protein purification and characterization
  - Bio-layer interferometry (BLI)
  - Nano differential scanning fluorimetry
  - Aggregation temperature (T_{agg}) determination
  - Immunogenicity studies
  - 288/330-hDDP4 transgenic mouse vaccinations and virus challenge experiments
  - Enzyme-linked immunosorbent assay (ELISA)
  - Competition ELISA
  - Generation of pseudoviruses
  - Pseudovirus neutralization assay
  - Negative stain electron microscopy (nsEM)
  - Ns-EMPEM
- QUANTIFICATION AND STATISTICAL ANALYSIS

SUPPLEMENTAL INFORMATION

Supplemental information can be found online at https://doi.org/10.1016/j.celrep.2024.115036.

Received: March 27, 2024
Revised: October 7, 2024
Accepted: November 14, 2024
Published: December 6, 2024

REFERENCES

1. Menachery, V.D., Yount, B.L., Debbink, K., Agnihothram, S., Gralinski, L.E., Plante, J.A., Graham, R.L., Scobey, T., Ge, X.-Y., Donaldson, E.F., et al. (2015). A SARS-like cluster of circulating bat coronaviruses shows potential for human emergence. Nat. Med. *21*, 1508–1513.
2. Menachery, V.D., Yount, B.L., Sims, A.C., Debbink, K., Agnihothram, S.S., Gralinski, L.E., Graham, R.L., Scobey, T., Plante, J.A., Royal, S.R., et al. (2016). SARS-like WIV1-CoV poised for human emergence. Proc. Natl. Acad. Sci. USA *113*, 3048–3053.
3. Zhou, P., Yang, X.-L., Wang, X.-G., Hu, B., Zhang, L., Zhang, W., Si, H.-R., Zhu, Y., Li, B., Huang, C.-L., et al. (2020). A pneumonia outbreak associated with a new coronavirus of probable bat origin. Nature *579*, 270–273.
4. Tse, L.V., Hou, Y.J., McFadden, E., Lee, R.E., Scobey, T.D., Leist, S.R., Martinez, D.R., Meganck, R.M., Schäfer, A., Yount, B.L., et al. (2023). A MERS-CoV antibody neutralizes a pre-emerging group 2c bat coronavirus. Sci. Transl. Med. *15*, eadg5567.
5. Vlasova, A.N., Diaz, A., Damtie, D., Xiu, L., Toh, T.-H., Lee, J.S.-Y., Saif, L.J., and Gray, G.C. (2022). Novel canine Coronavirus isolated from a hospitalized patient with pneumonia in east Malaysia. Clin. Infect. Dis. *74*, 446–454.
6. Lednicky, J.A., Tagliamonte, M.S., White, S.K., Elbadry, M.A., Alam, M.M., Stephenson, C.J., Bonny, T.S., Loeb, J.C., Telisma, T., Chavannes, S., et al. (2021). Independent infections of porcine deltacoronavirus among Haitian children. Nature *600*, 133–137.
7. Cassetti, M.C., Pierson, T.C., Patterson, L.J., Bok, K., DeRocco, A.J., Deschamps, A.M., Graham, B.S., Erbelding, E.J., and Fauci, A.S. (2022). Prototype Pathogen Approach for Vaccine and Monoclonal Antibody Development: A Critical Component of the NIAID Plan for Pandemic Preparedness. J. Infect. Dis. *227*, 1433–1441.
8. Ebrahim, S.H., Maher, A.D., Kanagasabai, U., Alfaraj, S.H., Alzahrani, N.A., Alqahtani, S.A., Assiri, A.M., and Memish, Z.A. (2021). MERS-CoV Confirmation among 6,873 suspected persons and relevant Epidemiologic and Clinical Features, Saudi Arabia — 2014 to 2019. eClinicalMedicine *41*, 101191. https://doi.org/10.1016/j.eclinm.2021.101191.
9. Arabi, Y.M., Arifi, A.A., Balkhy, H.H., Najm, H., Aldawood, A.S., Ghabashi, A., Hawa, H., Alothman, A., Khaldi, A., and Al Raiy, B. (2014). Clinical course and outcomes of critically ill patients with Middle East respiratory syndrome coronavirus infection. Ann. Intern. Med. *160*, 389–397.

10. Middle East respiratory syndrome: global summary and assessment of risk - 16 November 2022 https://apps.who.int/iris/bitstream/handle/10665/364525/WHO-MERS-RA-2022.1-eng.pdf.
11. Koch, T., Dahlke, C., Fathi, A., Kupke, A., Krähling, V., Okba, N.M.A., Halwe, S., Rohde, C., Eickmann, M., Volz, A., et al. (2020). Safety and immunogenicity of a modified vaccinia virus Ankara vector vaccine candidate for Middle East respiratory syndrome: an open-label, phase 1 trial. Lancet Infect. Dis. *20*, 827–838.
12. Folegatti, P.M., Bittaye, M., Flaxman, A., Lopez, F.R., Bellamy, D., Kupke, A., Mair, C., Makinson, R., Sheridan, J., Rohde, C., et al. (2020). Safety and immunogenicity of a candidate Middle East respiratory syndrome coronavirus viral-vectored vaccine: a dose-escalation, open-label, non-randomised, uncontrolled, phase 1 trial. Lancet Infect. Dis. *20*, 816–826.
13. Modjarrad, K., Roberts, C.C., Mills, K.T., Castellano, A.R., Paolino, K., Muthumani, K., Reuschel, E.L., Robb, M.L., Racine, T., Oh, M.-D., et al. (2019). Safety and immunogenicity of an anti-Middle East respiratory syndrome coronavirus DNA vaccine: a phase 1, open-label, single-arm, dose-escalation trial. Lancet Infect. Dis. *19*, 1013–1022.
14. Rey, F.A., and Lok, S.-M. (2018). Common Features of Enveloped Viruses and Implications for Immunogen Design for Next-Generation Vaccines. Cell *172*, 1319–1334.
15. Raj, V.S., Mou, H., Smits, S.L., Dekkers, D.H.W., Müller, M.A., Dijkman, R., Muth, D., Demmers, J.A.A., Zaki, A., Fouchier, R.A.M., et al. (2013). Dipeptidyl peptidase 4 is a functional receptor for the emerging human coronavirus-EMC. Nature *495*, 251–254.
16. Lu, G., Hu, Y., Wang, Q., Qi, J., Gao, F., Li, Y., Zhang, Y., Zhang, W., Yuan, Y., Bao, J., et al. (2013). Molecular basis of binding between novel human coronavirus MERS-CoV and its receptor CD26. Nature *500*, 227–231.
17. Wang, N., Shi, X., Jiang, L., Zhang, S., Wang, D., Tong, P., Guo, D., Fu, L., Cui, Y., Liu, X., et al. (2013). Structure of MERS-CoV spike receptor-binding domain complexed with human receptor DPP4. Cell Res. *23*, 986–993.
18. Li, W., Hulswit, R.J.G., Widjaja, I., Raj, V.S., McBride, R., Peng, W., Widagdo, W., Tortorici, M.A., van Dieren, B., Lang, Y., et al. (2017). Identification of sialic acid-binding function for the Middle East respiratory syndrome coronavirus spike glycoprotein. Proc. Natl. Acad. Sci. USA *114*, E8508–E8517.
19. Park, Y.-J., Walls, A.C., Wang, Z., Sauer, M.M., Li, W., Tortorici, M.A., Bosch, B.-J., DiMaio, F., and Veesler, D. (2019). Structures of MERS-CoV spike glycoprotein in complex with sialoside attachment receptors. Nat. Struct. Mol. Biol. *26*, 1151–1157.
20. Wang, L., Shi, W., Joyce, M.G., Modjarrad, K., Zhang, Y., Leung, K., Lees, C.R., Zhou, T., Yassine, H.M., Kanekiyo, M., et al. (2015). Evaluation of candidate vaccine approaches for MERS-CoV. Nat. Commun. *6*, 7712.
21. Widjaja, I., Wang, C., van Haperen, R., Gutiérrez-Álvarez, J., van Dieren, B., Okba, N.M.A., Raj, V.S., Li, W., Fernandez-Delgado, R., Grosveld, F., et al. (2019). Towards a solution to MERS: protective human monoclonal antibodies targeting different domains and functions of the MERS-coronavirus spike glycoprotein. Emerg. Microb. Infect. *8*, 516–530.
22. Corti, D., Zhao, J., Pedotti, M., Simonelli, L., Agnihothram, S., Fett, C., Fernandez-Rodriguez, B., Foglierini, M., Agatic, G., Vanzetta, F., et al. (2015). Prophylactic and postexposure efficacy of a potent human monoclonal antibody against MERS coronavirus. Proc. Natl. Acad. Sci. USA *112*, 10473–10478.
23. Jiang, L., Wang, N., Zuo, T., Shi, X., Poon, K.-M.V., Wu, Y., Gao, F., Li, D., Wang, R., Guo, J., et al. (2014). Potent neutralization of MERS-CoV by human neutralizing monoclonal antibodies to the viral spike glycoprotein. Sci. Transl. Med. *6*, 234ra59.
24. Li, Y., Wan, Y., Liu, P., Zhao, J., Lu, G., Qi, J., Wang, Q., Lu, X., Wu, Y., Liu, W., et al. (2015). A humanized neutralizing antibody against MERS-CoV targeting the receptor-binding domain of the spike protein. Cell Res. *25*, 1237–1249.
25. Zhou, H., Chen, Y., Zhang, S., Niu, P., Qin, K., Jia, W., Huang, B., Zhang, S., Lan, J., Zhang, L., et al. (2019). Structural definition of a neutralization epitope on the N-terminal domain of MERS-CoV spike glycoprotein. Nat. Commun. *10*, 3068.
26. Tang, X.-C., Agnihothram, S.S., Jiao, Y., Stanhope, J., Graham, R.L., Peterson, E.C., Avnir, Y., Tallarico, A.S.C., Sheehan, J., Zhu, Q., et al. (2014). Identification of human neutralizing antibodies against MERS-CoV and their role in virus adaptive evolution. Proc. Natl. Acad. Sci. USA *111*, E2018–E2026.
27. Wang, N., Rosen, O., Wang, L., Turner, H.L., Stevens, L.J., Corbett, K.S., Bowman, C.A., Pallesen, J., Shi, W., Zhang, Y., et al. (2019). Structural Definition of a Neutralization-Sensitive Epitope on the MERS-CoV S1-NTD. Cell Rep. *28*, 3395–3405.e6.
28. Hsieh, C.-L., Werner, A.P., Leist, S.R., Stevens, L.J., Falconer, E., Goldsmith, J.A., Chou, C.-W., Abiona, O.M., West, A., Westendorf, K., et al. (2021). Stabilized coronavirus spike stem elicits a broadly protective antibody. Cell Rep. *37*, 109929.
29. Sun, X., Yi, C., Zhu, Y., Ding, L., Xia, S., Chen, X., Liu, M., Gu, C., Lu, X., Fu, Y., et al. (2022). Neutralization mechanism of a human antibody with pan-coronavirus reactivity including SARS-CoV-2. Nat. Microbiol. *7*, 1063–1074.
30. Silva, R.P., Huang, Y., Nguyen, A.W., Hsieh, C.-L., Olaluwoye, O.S., Kaoud, T.S., Wilen, R.E., Qerqez, A.N., Park, J.-G., Khalil, A.M., et al. (2023). Identification of a conserved S2 epitope present on spike proteins from all highly pathogenic coronaviruses. Elife *12*, e83710. https://doi.org/10.7554/eLife.83710.
31. Sauer, M.M., Tortorici, M.A., Park, Y.-J., Walls, A.C., Homad, L., Acton, O.J., Bowen, J.E., Wang, C., Xiong, X., de van der Schueren, W., et al. (2021). Structural basis for broad coronavirus neutralization. Nat. Struct. Mol. Biol. *28*, 478–486.
32. Pinto, D., Sauer, M.M., Czudnochowski, N., Low, J.S., Tortorici, M.A., Housley, M.P., Noack, J., Walls, A.C., Bowen, J.E., Guarino, B., et al. (2021). Broad betacoronavirus neutralization by a stem helix-specific human antibody. Science *373*, 1109–1116.
33. Wang, C., van Haperen, R., Gutiérrez-Álvarez, J., Li, W., Okba, N.M.A., Albulescu, I., Widjaja, I., van Dieren, B., Fernandez-Delgado, R., Sola, I., et al. (2021). A conserved immunogenic and vulnerable site on the coronavirus spike protein delineated by cross-reactive monoclonal antibodies. Nat. Commun. *12*, 1715.
34. Zhou, P., Song, G., Liu, H., Yuan, M., He, W.-T., Beutler, N., Zhu, X., Tse, L.V., Martinez, D.R., Schäfer, A., et al. (2023). Broadly neutralizing anti-S2 antibodies protect against all three human betacoronaviruses that cause deadly disease. Immunity *56*, 669–686.e7.
35. Hurlburt, N.K., Homad, L.J., Sinha, I., Jennewein, M.F., MacCamy, A.J., Wan, Y.-H., Boonyaratanakornkit, J., Sholukh, A.M., Jackson, A.M., Zhou, P., et al. (2022). Structural definition of a pan-sarbecovirus neutralizing epitope on the spike S2 subunit. Commun. Biol. *5*, 342.
36. Low, J.S., Jerak, J., Tortorici, M.A., McCallum, M., Pinto, D., Cassotta, A., Foglierini, M., Mele, F., Abdelnabi, R., Weynand, B., et al. (2022). ACE2-binding exposes the SARS-CoV-2 fusion peptide to broadly neutralizing coronavirus antibodies. Science *377*, 735–742.
37. Rodon, J., Mykytyn, A.Z., Cantero, G., Albulescu, I.C., Bosch, B.-J., Brix, A., Audonnet, J.-C., Bensaid, A., Vergara-Alert, J., Haagmans, B.L., and Segalés, J. (2022). Protective efficacy of an RBD-based Middle East respiratory syndrome coronavirus (MERS-CoV) particle vaccine in llamas. One Health Outlook *4*, 12.
38. Okba, N.M.A., Widjaja, I., van Dieren, B., Aebischer, A., van Amerongen, G., de Waal, L., Stittelaar, K.J., Schipper, D., Martina, B., van den Brand, J.M.A., et al. (2020). Particulate multivalent presentation of the receptor binding domain induces protective immune responses against MERS-CoV. Emerg. Microb. Infect. *9*, 1080–1091.
39. Hutchinson, G.B., Abiona, O.M., Ziwawo, C.T., Werner, A.P., Ellis, D., Tsybovsky, Y., Leist, S.R., Palandjian, C., West, A., Fritch, E.J., et al. (2023). Nanoparticle display of prefusion coronavirus spike elicits

S1-focused cross-reactive antibody response against diverse coronavirus subgenera. Nat. Commun. *14*, 6195.

40. Pallesen, J., Wang, N., Corbett, K.S., Wrapp, D., Kirchdoerfer, R.N., Turner, H.L., Cottrell, C.A., Becker, M.M., Wang, L., Shi, W., et al. (2017). Immunogenicity and structures of a rationally designed prefusion MERS-CoV spike antigen. Proc. Natl. Acad. Sci. USA *114*, E7348–E7357.
41. Coleman, C.M., Liu, Y.V., Mu, H., Taylor, J.K., Massare, M., Flyer, D.C., Smith, G.E., and Frieman, M.B. (2014). Purified coronavirus spike protein nanoparticles induce coronavirus neutralizing antibodies in mice. Vaccine *32*, 3169–3174.
42. Corbett, K.S., Edwards, D.K., Leist, S.R., Abiona, O.M., Boyoglu-Barnum, S., Gillespie, R.A., Himansu, S., Schäfer, A., Ziwawo, C.T., DiPiazza, A.T., et al. (2020). SARS-CoV-2 mRNA vaccine design enabled by prototype pathogen preparedness. Nature *586*, 567–571.
43. Walls, A.C., Park, Y.-J., Tortorici, M.A., Wall, A., McGuire, A.T., and Veesler, D. (2020). Structure, Function, and Antigenicity of the SARS-CoV-2 Spike Glycoprotein. Cell *183*, 1735.
44. Wrapp, D., Wang, N., Corbett, K.S., Goldsmith, J.A., Hsieh, C.-L., Abiona, O., Graham, B.S., and McLellan, J.S. (2020). Cryo-EM Structure of the 2019-nCoV Spike in the Prefusion Conformation. Preprint at bioRxiv. https://doi.org/10.1101/2020.02.11.944462.
45. Pardi, N., and Weissman, D. (2020). Development of vaccines and antivirals for combating viral pandemics. Nat. Biomed. Eng. *4*, 1128–1133.
46. Karikó, K., Buckstein, M., Ni, H., and Weissman, D. (2005). Suppression of RNA recognition by Toll-like receptors: the impact of nucleoside modification and the evolutionary origin of RNA. Immunity *23*, 165–175.
47. Song, J.Y., Choi, W.S., Heo, J.Y., Kim, E.J., Lee, J.S., Jung, D.S., Kim, S.-W., Park, K.-H., Eom, J.S., Jeong, S.J., et al. (2023). Immunogenicity and safety of SARS-CoV-2 recombinant protein nanoparticle vaccine GBP510 adjuvanted with AS03: interim results of a randomised, active-controlled, observer-blinded, phase 3 trial. eClinicalMedicine *64*, 102140. https://doi.org/10.1016/j.eclinm.2023.102140.
48. Song, J.Y., Choi, W.S., Heo, J.Y., Lee, J.S., Jung, D.S., Kim, S.-W., Park, K.-H., Eom, J.S., Jeong, S.J., Lee, J., et al. (2022). Safety and immunogenicity of a SARS-CoV-2 recombinant protein nanoparticle vaccine (GBP510) adjuvanted with AS03: A randomised, placebo-controlled, observer-blinded phase 1/2 trial. EClinicalMedicine *51*, 101569.
49. Ols, S., Lenart, K., Arcoverde Cerveira, R., Miranda, M.C., Brunette, N., Kochmann, J., Corcoran, M., Skotheim, R., Philomin, A., Cagigi, A., et al. (2023). Multivalent antigen display on nanoparticle immunogens increases B cell clonotype diversity and neutralization breadth to pneumoviruses. Immunity *56*, 2425–2441.e14.
50. Marcandalli, J., Fiala, B., Ols, S., Perotti, M., de van der Schueren, W., Snijder, J., Hodge, E., Benhaim, M., Ravichandran, R., Carter, L., et al. (2019). Induction of Potent Neutralizing Antibody Responses by a Designed Protein Nanoparticle Vaccine for Respiratory Syncytial Virus. Cell *176*, 1420–1431.e17.
51. Perotti, M., Marcandalli, J., Demurtas, D., Sallusto, F., and Perez, L. (2020). Rationally designed Human Cytomegalovirus gB nanoparticle vaccine with improved immunogenicity. PLoS Pathog. *16*, e1009169.
52. Brouwer, P.J.M., Antanasijevic, A., Berndsen, Z., Yasmeen, A., Fiala, B., Bijl, T.P.L., Bontjer, I., Bale, J.B., Sheffler, W., Allen, J.D., et al. (2019). Enhancing and shaping the immunogenicity of native-like HIV-1 envelope trimers with a two-component protein nanoparticle. Nat. Commun. *10*, 4272.
53. Antanasijevic, A., Ueda, G., Brouwer, P.J.M., Copps, J., Huang, D., Allen, J.D., Cottrell, C.A., Yasmeen, A., Sewall, L.M., Bontjer, I., et al. (2020). Structural and functional evaluation of de novo-designed, two-component nanoparticle carriers for HIV Env trimer immunogens. PLoS Pathog. *16*, e1008665.
54. Sliepen, K., Radić, L., Capella-Pujol, J., Watanabe, Y., Zon, I., Chumbe, A., Lee, W.-H., de Gast, M., Koopsen, J., Koekkoek, S., et al. (2022). Induction of cross-neutralizing antibodies by a permuted hepatitis C virus glycoprotein nanoparticle vaccine candidate. Nat. Commun. *13*, 7271.
55. Brouwer, P.J.M., Antanasijevic, A., Ronk, A.J., Müller-Kräuter, H., Watanabe, Y., Claireaux, M., Perrett, H.R., Bijl, T.P.L., Grobben, M., Umotoy, J.C., et al. (2022). Lassa virus glycoprotein nanoparticles elicit neutralizing antibody responses and protection. Cell Host Microbe *30*, 1759–1772.e12.
56. Boyoglu-Barnum, S., Ellis, D., Gillespie, R.A., Hutchinson, G.B., Park, Y.-J., Moin, S.M., Acton, O.J., Ravichandran, R., Murphy, M., Pettie, D., et al. (2021). Quadrivalent influenza nanoparticle vaccines induce broad protection. Nature *592*, 623–628.
57. Kang, Y.-F., Sun, C., Zhuang, Z., Yuan, R.-Y., Zheng, Q., Li, J.-P., Zhou, P.-P., Chen, X.-C., Liu, Z., Zhang, X., et al. (2021). Rapid Development of SARS-CoV-2 Spike Protein Receptor-Binding Domain Self-Assembled Nanoparticle Vaccine Candidates. ACS Nano *15*, 2738–2752.
58. Nguyen, B., and Tolia, N.H. (2021). Protein-based antigen presentation platforms for nanoparticle vaccines. NPJ Vaccines *6*, 70.
59. Read, B.J., Won, L., Kraft, J.C., Sappington, I., Aung, A., Wu, S., Bals, J., Chen, C., Lee, K.K., Lingwood, D., et al. (2022). Mannose-binding lectin and complement mediate follicular localization and enhanced immunogenicity of diverse protein nanoparticle immunogens. Cell Rep. *38*, 110217.
60. Martin, J.T., Cottrell, C.A., Antanasijevic, A., Carnathan, D.G., Cossette, B.J., Enemuo, C.A., Gebru, E.H., Choe, Y., Viviano, F., Fischinger, S., et al. (2020). Targeting HIV Env immunogens to B cell follicles in nonhuman primates through immune complex or protein nanoparticle formulations. NPJ Vaccines *5*, 72.
61. Bale, J.B., Gonen, S., Liu, Y., Sheffler, W., Ellis, D., Thomas, C., Cascio, D., Yeates, T.O., Gonen, T., King, N.P., and Baker, D. (2016). Accurate design of megadalton-scale two-component icosahedral protein complexes. Science *353*, 389–394.
62. Walls, A.C., Fiala, B., Schäfer, A., Wrenn, S., Pham, M.N., Murphy, M., Tse, L.V., Shehata, L., O'Connor, M.A., Chen, C., et al. (2020). Elicitation of Potent Neutralizing Antibody Responses by Designed Protein Nanoparticle Vaccines for SARS-CoV-2. Cell *183*, 1367–1382.e17.
63. Grigoryan, L., Lee, A., Walls, A.C., Lai, L., Franco, B., Arunachalam, P.S., Feng, Y., Luo, W., Vanderheiden, A., Floyd, K., et al. (2022). Adjuvanting a subunit SARS-CoV-2 vaccine with clinically relevant adjuvants induces durable protection in mice. NPJ Vaccines *7*, 55.
64. Arunachalam, P.S., Walls, A.C., Golden, N., Atyeo, C., Fischinger, S., Li, C., Aye, P., Navarro, M.J., Lai, L., Edara, V.V., et al. (2021). Adjuvanting a subunit COVID-19 vaccine to induce protective immunity. Nature *594*, 253–258.
65. Walls, A.C., Miranda, M.C., Schäfer, A., Pham, M.N., Greaney, A., Arunachalam, P.S., Navarro, M.-J., Tortorici, M.A., Rogers, K., O'Connor, M.A., et al. (2021). Elicitation of broadly protective sarbecovirus immunity by receptor-binding domain nanoparticle vaccines. Cell *184*, 5432–5447.e16.
66. Ueda, G., Antanasijevic, A., Fallas, J.A., Sheffler, W., Copps, J., Ellis, D., Hutchinson, G.B., Moyer, A., Yasmeen, A., Tsybovsky, Y., et al. (2020). Tailored design of protein nanoparticle scaffolds for multivalent presentation of viral glycoprotein antigens. Elife *9*, e57659.
67. Brinkkemper, M., Veth, T.S., Brouwer, P.J.M., Turner, H., Poniman, M., Burger, J.A., Bouhuijs, J.H., Olijhoek, W., Bontjer, I., Snitselaar, J.L., et al. (2022). Co-display of diverse spike proteins on nanoparticles broadens sarbecovirus neutralizing antibody responses. iScience *25*, 105649.
68. Brouwer, P.J.M., Brinkkemper, M., Maisonnasse, P., Dereuddre-Bosquet, N., Grobben, M., Claireaux, M., de Gast, M., Marlin, R., Chesnais, V., Diry, S., et al. (2021). Two-component spike nanoparticle vaccine protects macaques from SARS-CoV-2 infection. Cell *184*, 1188–1200.e19.

69. Kang, Y.-F., Sun, C., Sun, J., Xie, C., Zhuang, Z., Xu, H.-Q., Liu, Z., Liu, Y.-H., Peng, S., Yuan, R.-Y., et al. (2022). Quadrivalent mosaic HexaPro-bearing nanoparticle vaccine protects against infection of SARS-CoV-2 variants. Nat. Commun. *13*, 2674.

70. Zhang, S., Jia, W., Zeng, J., Li, M., Wang, Z., Zhou, H., Zhang, L., and Wang, X. (2022). Cryoelectron microscopy structures of a human neutralizing antibody bound to MERS-CoV spike glycoprotein. Front. Microbiol. *13*, 988298.

71. Seydoux, E., Homad, L.J., MacCamy, A.J., Parks, K.R., Hurlburt, N.K., Jennewein, M.F., Akins, N.R., Stuart, A.B., Wan, Y.-H., Feng, J., et al. (2020). Analysis of a SARS-CoV-2-Infected Individual Reveals Development of Potent Neutralizing Antibodies with Limited Somatic Mutation. Immunity *53*, 98–105.e5.

72. Hsieh, C.-L., Goldsmith, J.A., Schaub, J.M., DiVenere, A.M., Kuo, H.-C., Javanmardi, K., Le, K.C., Wrapp, D., Lee, A.G., Liu, Y., et al. (2020). Structure-based design of prefusion-stabilized SARS-CoV-2 spikes. Science *369*, 1501–1505.

73. Bianchi, M., Turner, H.L., Nogal, B., Cottrell, C.A., Oyen, D., Pauthner, M., Bastidas, R., Nedellec, R., McCoy, L.E., Wilson, I.A., et al. (2018). Electron-Microscopy-Based Epitope Mapping Defines Specificities of Polyclonal Antibodies Elicited during HIV-1 BG505 Envelope Trimer Immunization. Immunity *49*, 288–300.e8.

74. Bangaru, S., Antanasijevic, A., Kose, N., Sewall, L.M., Jackson, A.M., Suryadevara, N., Zhan, X., Torres, J.L., Copps, J., de la Peña, A.T., et al. (2022). Structural mapping of antibody landscapes to human betacoronavirus spike proteins. Sci. Adv. *8*, eabn2911.

75. Malhi, H., Homad, L.J., Wan, Y.-H., Poudel, B., Fiala, B., Borst, A.J., Wang, J.Y., Walkey, C., Price, J., Wall, A., et al. (2022). Immunization with a self-assembling nanoparticle vaccine displaying EBV gH/gL protects humanized mice against lethal viral challenge. Cell Rep. Med. *3*, 100658.

76. Kato, Y., Abbott, R.K., Freeman, B.L., Haupt, S., Groschel, B., Silva, M., Menis, S., Irvine, D.J., Schief, W.R., and Crotty, S. (2020). Multifaceted Effects of Antigen Valency on B Cell Response Composition and Differentiation In Vivo. Immunity *53*, 548–563.e8.

77. Ellis, D., Brunette, N., Crawford, K.H.D., Walls, A.C., Pham, M.N., Chen, C., Herpoldt, K.-L., Fiala, B., Murphy, M., Pettie, D., et al. (2021). Stabilization of the SARS-CoV-2 Spike receptor-binding domain using deep mutational scanning and structure-based design. Front Immunol. *12*, 710263.

78. Joyce, M.G., Zhang, B., Ou, L., Chen, M., Chuang, G.-Y., Druz, A., Kong, W.-P., Lai, Y.-T., Rundlet, E.J., Tsybovsky, Y., et al. (2016). Iterative structure-based improvement of a fusion-glycoprotein vaccine against RSV. Nat. Struct. Mol. Biol. *23*, 811–820.

79. del Moral-Sánchez, I., Russell, R.A., Schermer, E.E., Cottrell, C.A., Allen, J.D., Torrents de la Peña, A., LaBranche, C.C., Kumar, S., Crispin, M., Ward, A.B., et al. (2022). High thermostability improves neutralizing antibody responses induced by native-like HIV-1 envelope trimers. npj Vaccines *7*, 1–12.

80. Dosey, A., Ellis, D., Boyoglu-Barnum, S., Syeda, H., Saunders, M., Watson, M., Kraft, J.C., Pham, M.N., Guttman, M., Lee, K.K., et al. (2023). Combinatorial Immune Refocusing within the Influenza Hemagglutinin Head Elicits Cross-Neutralizing Antibody Responses.. Preprint at bioRxiv. https://doi.org/10.1101/2023.05.23.541996.

81. Ellis, D., Dosey, A., Boyoglu-Barnum, S., Park, Y.-J., Gillespie, R., Syeda, H., Tsybovsky, Y., Murphy, M., Pettie, D., Matheson, N., et al. (2023). Antigen spacing on protein nanoparticles influences antibody responses to vaccination. Preprint at bioRxiv. https://doi.org/10.1101/2023.05.23.541980.

82. McLeod, B., Mabrouk, M.T., Miura, K., Ravichandran, R., Kephart, S., Hailemariam, S., Pham, T.P., Semesi, A., Kucharska, I., Kundu, P., et al. (2022). Vaccination with a structure-based stabilized version of malarial antigen Pfs48/45 elicits ultra-potent transmission-blocking antibody responses. Immunity *55*, 1680–1692.e8.

83. Kanekiyo, M., Bu, W., Joyce, M.G., Meng, G., Whittle, J.R.R., Baxa, U., Yamamoto, T., Narpala, S., Todd, J.-P., Rao, S.S., et al. (2015). Rational Design of an Epstein-Barr Virus Vaccine Targeting the Receptor-Binding Site. Cell *162*, 1090–1100.

84. Kanekiyo, M., Joyce, M.G., Gillespie, R.A., Gallagher, J.R., Andrews, S.F., Yassine, H.M., Wheatley, A.K., Fisher, B.E., Ambrozak, D.R., Creanga, A., et al. (2019). Mosaic nanoparticle display of diverse influenza virus hemagglutinins elicits broad B cell responses. Nat. Immunol. *20*, 362–372.

85. Jardine, J., Julien, J.-P., Menis, S., Ota, T., Kalyuzhniy, O., McGuire, A., Sok, D., Huang, P.-S., MacPherson, S., Jones, M., et al. (2013). Rational HIV immunogen design to target specific germline B cell receptors. Science *340*, 711–716.

86. Cerutti, G., Guo, Y., Zhou, T., Gorman, J., Lee, M., Rapp, M., Reddem, E.R., Yu, J., Bahna, F., Bimela, J., et al. (2021). Potent SARS-CoV-2 neutralizing antibodies directed against spike N-terminal domain target a single supersite. Cell Host Microbe *29*, 819–833.e7.

87. Liu, L., Wang, P., Nair, M.S., Yu, J., Rapp, M., Wang, Q., Luo, Y., Chan, J.F.-W., Sahi, V., Figueroa, A., et al. (2020). Potent neutralizing antibodies against multiple epitopes on SARS-CoV-2 spike. Nature *584*, 450–456.

88. McCallum, M., De Marco, A., Lempp, F.A., Tortorici, M.A., Pinto, D., Walls, A.C., Beltramello, M., Chen, A., Liu, Z., Zatta, F., et al. (2021). N-terminal domain antigenic mapping reveals a site of vulnerability for SARS-CoV-2. Cell *184*, 2332–2347.e16.

89. Starr, T.N., Czudnochowski, N., Liu, Z., Zatta, F., Park, Y.-J., Addetia, A., Pinto, D., Beltramello, M., Hernandez, P., Greaney, A.J., et al. (2021). SARS-CoV-2 RBD antibodies that maximize breadth and resistance to escape. Nature *597*, 97–102.

90. Walls, A.C., Xiong, X., Park, Y.-J., Tortorici, M.A., Snijder, J., Quispe, J., Cameroni, E., Gopal, R., Dai, M., Lanzavecchia, A., et al. (2020). Unexpected Receptor Functional Mimicry Elucidates Activation of Coronavirus Fusion. Cell *183*, 1732.

91. Premkumar, L., Segovia-Chumbez, B., Jadi, R., Martinez, D.R., Raut, R., Markmann, A., Cornaby, C., Bartelt, L., Weiss, S., Park, Y., et al. (2020). The receptor binding domain of the viral spike protein is an immunodominant and highly specific target of antibodies in SARS-CoV-2 patients. Sci. Immunol. *5*, eabc8413. https://doi.org/10.1126/sciimmunol.abc8413.

92. Piccoli, L., Park, Y.-J., Tortorici, M.A., Czudnochowski, N., Walls, A.C., Beltramello, M., Silacci-Fregni, C., Pinto, D., Rosen, L.E., Bowen, J.E., et al. (2020). Mapping Neutralizing and Immunodominant Sites on the SARS-CoV-2 Spike Receptor-Binding Domain by Structure-Guided High-Resolution Serology. Cell *183*, 1024–1042.e21.

93. Wong, A.H.M., Tomlinson, A.C.A., Zhou, D., Satkunarajah, M., Chen, K., Sharon, C., Desforges, M., Talbot, P.J., and Rini, J.M. (2017). Receptor-binding loops in alphacoronavirus adaptation and evolution. Nat. Commun. *8*, 1735.

94. Addetia, A., Stewart, C., Seo, A.J., Sprouse, K.R., Asiri, A.Y., Al-Mozaini, M., Memish, Z.A., Alshukairi, A.N., and Veesler, D. (2024). Mapping immunodominant sites on the MERS-CoV spike glycoprotein targeted by infection-elicited antibodies in humans. Cell Rep. *43*, 114530.

95. Huo, J., Zhao, Y., Ren, J., Zhou, D., Duyvesteyn, H.M.E., Ginn, H.M., Carrique, L., Malinauskas, T., Ruza, R.R., Shah, P.N.M., et al. (2020). Neutralization of SARS-CoV-2 by Destruction of the Prefusion Spike. Cell Host Microbe *28*, 497.

96. Stamatatos, L., Czartoski, J., Wan, Y.-H., Homad, L.J., Rubin, V., Glantz, H., Neradilek, M., Seydoux, E., Jennewein, M.F., MacCamy, A.J., et al. (2021). mRNA vaccination boosts cross-variant neutralizing antibodies elicited by SARS-CoV-2 infection. Science *372*, 1413–1418.

97. Greaney, A.J., Loes, A.N., Gentles, L.E., Crawford, K.H.D., Starr, T.N., Malone, K.D., Chu, H.Y., and Bloom, J.D. (2021). Antibodies elicited by mRNA-1273 vaccination bind more broadly to the receptor binding domain than do those from SARS-CoV-2 infection. Sci. Transl. Med. *13*, eabi9915. https://doi.org/10.1126/scitranslmed.abi9915.

98. Bowen, J.E., Park, Y.-J., Stewart, C., Brown, J.T., Sharkey, W.K., Walls, A.C., Joshi, A., Sprouse, K.R., McCallum, M., Tortorici, M.A., et al. (2022). SARS-CoV-2 spike conformation determines plasma neutralizing activity elicited by a wide panel of human vaccines. Sci. Immunol. *7*, eadf1421.

99. Robbiani, D.F., Gaebler, C., Muecksch, F., Lorenzi, J.C.C., Wang, Z., Cho, A., Agudelo, M., Barnes, C.O., Gazumyan, A., Finkin, S., et al. (2020). Convergent antibody responses to SARS-CoV-2 in convalescent individuals. Nature *584*, 437–442.

100. Douglas, M.G., Kocher, J.F., Scobey, T., Baric, R.S., and Cockrell, A.S. (2018). Adaptive evolution influences the infectious dose of MERS-CoV necessary to achieve severe respiratory disease. Virology *517*, 98–107.

101. Cockrell, A.S., Yount, B.L., Scobey, T., Jensen, K., Douglas, M., Beall, A., Tang, X.-C., Marasco, W.A., Heise, M.T., and Baric, R.S. (2016). A mouse model for MERS coronavirus-induced acute respiratory distress syndrome. Nat. Microbiol. *2*, 16226.

102. Dalvie, N.C., Rodriguez-Aponte, S.A., Hartwell, B.L., Tostanoski, L.H., Biedermann, A.M., Crowell, L.E., Kaur, K., Kumru, O.S., Carter, L., Yu, J., et al. (2021). Engineered SARS-CoV-2 receptor binding domain improves manufacturability in yeast and immunogenicity in mice. Proc. Natl. Acad. Sci. USA *118*, e2106845118.

103. Tan, T.K., Rijal, P., Rahikainen, R., Keeble, A.H., Schimanski, L., Hussain, S., Harvey, R., Hayes, J.W.P., Edwards, J.C., McLean, R.K., et al. (2021). A COVID-19 vaccine candidate using SpyCatcher multimerization of the SARS-CoV-2 spike protein receptor-binding domain induces potent neutralising antibody responses. Nat. Commun. *12*, 542.

104. Cohen, A.A., Gnanapragasam, P.N.P., Lee, Y.E., Hoffman, P.R., Ou, S., Kakutani, L.M., Keeffe, J.R., Wu, H.-J., Howarth, M., West, A.P., et al. (2021). Mosaic nanoparticles elicit cross-reactive immune responses to zoonotic coronaviruses in mice. Science *371*, 735–741.

105. King, H.A.D., Joyce, M.G., Lakhal-Naouar, I., Ahmed, A., Cincotta, C.M., Subra, C., Peachman, K.K., Hack, H.R., Chen, R.E., Thomas, P.V., et al. (2021). Efficacy and breadth of adjuvanted SARS-CoV-2 receptor-binding domain nanoparticle vaccine in macaques. Proc. Natl. Acad. Sci. USA *118*, e2106433118. https://doi.org/10.1073/pnas.2106433118.

106. Saunders, K.O., Lee, E., Parks, R., Martinez, D.R., Li, D., Chen, H., Edwards, R.J., Gobeil, S., Barr, M., Mansouri, K., et al. (2021). Neutralizing antibody vaccine for pandemic and pre-emergent coronaviruses. Nature *594*, 553–559.

107. Weidenbacher, P.A.-B., Sanyal, M., Friedland, N., Tang, S., Arunachalam, P.S., Hu, M., Kumru, O.S., Morris, M.K., Fontenot, J., Shirreff, L., et al. (2023). A ferritin-based COVID-19 nanoparticle vaccine that elicits robust, durable, broad-spectrum neutralizing antisera in non-human primates. Nat. Commun. *14*, 2149.

108. Fougeroux, C., Goksøyr, L., Idorn, M., Soroka, V., Myeni, S.K., Dagil, R., Janitzek, C.M., Søgaard, M., Aves, K.-L., Horsted, E.W., et al. (2021). Capsid-like particles decorated with the SARS-CoV-2 receptor-binding domain elicit strong virus neutralization activity. Nat. Commun. *12*, 324.

109. Bangaru, S., Ozorowski, G., Turner, H.L., Antanasijevic, A., Huang, D., Wang, X., Torres, J.L., Diedrich, J.K., Tian, J.-H., Portnoff, A.D., et al. (2020). Structural analysis of full-length SARS-CoV-2 spike protein from an advanced vaccine candidate. Science *370*, 1089–1094.

110. Martinez, D.R., Schäfer, A., Gavitt, T.D., Mallory, M.L., Lee, E., Catanzaro, N.J., Chen, H., Gully, K., Scobey, T., Koratagere, P., et al. (2023). Vaccine-mediated protection against Merbecovirus and Sarbecovirus challenge in mice. Cell Rep. *42*, 113248.

111. Cohen, A.A., van Doremalen, N., Greaney, A.J., Andersen, H., Sharma, A., Starr, T.N., Keeffe, J.R., Fan, C., Schulz, J.E., Gnanapragasam, P.N.P., et al. (2022). Mosaic RBD nanoparticles protect against challenge by diverse sarbecoviruses in animal models. Science *377*, eabq0839.

112. Zhang, Y., Sun, J., Zheng, J., Li, S., Rao, H., Dai, J., Zhang, Z., Wang, Y., Liu, D., Chen, Z., et al. (2024). Mosaic RBD Nanoparticles Elicit Protective Immunity Against Multiple Human Coronaviruses in Animal Models. Adv. Sci. *11*, e2303366.

113. Pierre, C.N., Adams, L.E., Anasti, K., Goodman, D., Stanfield-Oakley, S., Powers, J.M., Li, D., Rountree, W., Wang, Y., Edwards, R.J., et al. (2023). Non-neutralizing SARS-CoV-2 N-terminal domain antibodies protect mice against severe disease using Fc-mediated effector functions. Preprint at bioRxiv. https://doi.org/10.1101/2023.07.25.550460.

114. Mackin, S.R., Desai, P., Whitener, B.M., Karl, C.E., Liu, M., Baric, R.S., Edwards, D.K., Chicz, T.M., McNamara, R.P., Alter, G., and Diamond, M.S. (2023). Fc-γR-dependent antibody effector functions are required for vaccine-mediated protection against antigen-shifted variants of SARS-CoV-2. Nat. Microbiol. *8*, 569–580.

115. Addetia, A., Piccoli, L., Case, J.B., Park, Y.-J., Beltramello, M., Guarino, B., Dang, H., de Melo, G.D., Pinto, D., Sprouse, K., et al. (2023). Neutralization, effector function and immune imprinting of Omicron variants. Nature *621*, 592–601.

116. Winkler, E.S., Gilchuk, P., Yu, J., Bailey, A.L., Chen, R.E., Chong, Z., Zost, S.J., Jang, H., Huang, Y., Allen, J.D., et al. (2021). Human neutralizing antibodies against SARS-CoV-2 require intact Fc effector functions for optimal therapeutic protection. Cell *184*, 1804–1820.e16.

117. Schäfer, A., Muecksch, F., Lorenzi, J.C.C., Leist, S.R., Cipolla, M., Bournazos, S., Schmidt, F., Maison, R.M., Gazumyan, A., Martinez, D.R., et al. (2021). Antibody potency, effector function, and combinations in protection and therapy for SARS-CoV-2 infection in vivo. J. Exp. Med. *218*, e20201993. https://doi.org/10.1084/jem.20201993.

118. Corti, D., Purcell, L.A., Snell, G., and Veesler, D. (2021). Tackling COVID-19 with neutralizing monoclonal antibodies. Cell *184*, 4593–4595.

119. Barnes, C.O., Jette, C.A., Abernathy, M.E., Dam, K.-M.A., Esswein, S.R., Gristick, H.B., Malyutin, A.G., Sharaf, N.G., Huey-Tubman, K.E., Lee, Y.E., et al. (2020). SARS-CoV-2 neutralizing antibody structures inform therapeutic strategies. Nature *588*, 682–687.

120. Wang, L., Shi, W., Chappell, J.D., Joyce, M.G., Zhang, Y., Kanekiyo, M., Becker, M.M., van Doremalen, N., Fischer, R., Wang, N., et al. (2018). Importance of Neutralizing Monoclonal Antibodies Targeting Multiple Antigenic Sites on the Middle East Respiratory Syndrome Coronavirus Spike Glycoprotein To Avoid Neutralization Escape. J. Virol. *92*, e02002-17. https://doi.org/10.1128/JVI.02002-17.

121. Chen, Y., Lu, S., Jia, H., Deng, Y., Zhou, J., Huang, B., Yu, Y., Lan, J., Wang, W., Lou, Y., et al. (2017). A novel neutralizing monoclonal antibody targeting the N-terminal domain of the MERS-CoV spike protein. Emerg. Microb. Infect. *6*, e60.

122. McCallum, M., Bassi, J., De Marco, A., Chen, A., Walls, A.C., Di Iulio, J., Tortorici, M.A., Navarro, M.-J., Silacci-Fregni, C., Saliba, C., et al. (2021). SARS-CoV-2 immune evasion by the B.1.427/B.1.429 variant of concern. Science *373*, 648–654.

123. McCallum, M., Walls, A.C., Sprouse, K.R., Bowen, J.E., Rosen, L.E., Dang, H.V., De Marco, A., Franko, N., Tilles, S.W., Logue, J., et al. (2021). Molecular basis of immune evasion by the Delta and Kappa SARS-CoV-2 variants. Science *374*, 1621–1626.

124. McCallum, M., Czudnochowski, N., Rosen, L.E., Zepeda, S.K., Bowen, J.E., Walls, A.C., Hauser, K., Joshi, A., Stewart, C., Dillen, J.R., et al. (2022). Structural basis of SARS-CoV-2 Omicron immune evasion and receptor engagement. Science *375*, 864–868.

125. Wargacki, A.J., Wörner, T.P., van de Waterbeemd, M., Ellis, D., Heck, A.J.R., and King, N.P. (2021). Complete and cooperative in vitro assembly of computationally designed self-assembling protein nanomaterials. Nat. Commun. *12*, 883.

126. Aung, A., Cui, A., Maiorino, L., Amini, A.P., Gregory, J.R., Bukenya, M., Zhang, Y., Lee, H., Cottrell, C.A., Morgan, D.M., et al. (2023). Low protease activity in B cell follicles promotes retention of intact antigens after immunization. Science *379*, eabn8934.

127. Powell, A.E., Caruso, H., Park, S., Chen, J.-L., O'Rear, J., Ferrer, B.J., Walker, A., Bruening, A., Hartwig, A., Ahyong, V., et al. (2024). A stabilized MERS-CoV spike ferritin nanoparticle vaccine elicits robust and protective neutralizing antibody responses. Preprint at bioRxiv. https://doi.org/10.1101/2024.07.01.601243.

128. Tokatlian, T., Read, B.J., Jones, C.A., Kulp, D.W., Menis, S., Chang, J.Y.H., Steichen, J.M., Kumari, S., Allen, J.D., Dane, E.L., et al. (2019). Innate immune recognition of glycans targets HIV nanoparticle immunogens to germinal centers. Science *363*, 649–654.

129. Dosey, A., Ellis, D., Boyoglu-Barnum, S., Syeda, H., Saunders, M., Watson, M.J., Kraft, J.C., Pham, M.N., Guttman, M., Lee, K.K., et al. (2023). Combinatorial immune refocusing within the influenza hemagglutinin RBD improves cross-neutralizing antibody responses. Cell Rep. *42*, 113553.

130. Brouwer, P.J.M., Perrett, H.R., Beaumont, T., Nijhuis, H., Kruijer, S., Burger, J.A., Bontjer, I., Lee, W.-H., Ferguson, J.A., Schauflinger, M., et al. (2024). Defining bottlenecks and opportunities for Lassa virus neutralization by structural profiling of vaccine-induced polyclonal antibody responses. Cell Rep. *43*, 114708.

131. Turner, H.L., Andrabi, R., Cottrell, C.A., Richey, S.T., Song, G., Callaghan, S., Anzanello, F., Moyer, T.J., Abraham, W., Melo, M., et al. (2021). Disassembly of HIV envelope glycoprotein trimer immunogens is driven by antibodies elicited via immunization. Sci. Adv. *7*, eabh2791.

132. Zhao, J., Wan, W., Yu, K., Lemey, P., Pettersson, J.H.-O., Bi, Y., Lu, M., Li, X., Chen, Z., Zheng, M., et al. (2024). Farmed fur animals harbour viruses with zoonotic spillover potential. Nature *634*, 228–233.

133. Catanzaro, N.J., Wu, Z., Fan, C., Schäfer, A., Yount, B.L., Bjorkman, P.J., Baric, R., and Letko, M. (2024). ACE2 from *Pipistrellus abramus* bats is a receptor for HKU5 coronaviruses. Preprint at bioRxiv. https://doi.org/10.1101/2024.03.13.584892.

134. Speranskaya, A.S., Artiushin, I.V., Samoilov, A.E., Korneenko, E.V., Khabudaev, K.V., Ilina, E.N., Yusefovich, A.P., Safonova, M.V., Dolgova, A.S., Gladkikh, A.S., et al. (2023). Identification and genetic characterization of MERS-related Coronavirus isolated from Nathusius' pipistrelle (*Pipistrellus nathusii*) near zvenigorod (Moscow Region, Russia). Int. J. Environ. Res. Publ. Health *20*, 3702. https://doi.org/10.3390/ijerph20043702.

135. Punjani, A., Rubinstein, J.L., Fleet, D.J., and Brubaker, M.A. (2017). cryoSPARC: algorithms for rapid unsupervised cryo-EM structure determination. Nat. Methods *14*, 290–296.

136. Pettersen, E.F., Goddard, T.D., Huang, C.C., Couch, G.S., Greenblatt, D.M., Meng, E.C., and Ferrin, T.E. (2004). UCSF Chimera–a visualization system for exploratory research and analysis. J. Comput. Chem. *25*, 1605–1612.

137. Goddard, T.D., Huang, C.C., Meng, E.C., Pettersen, E.F., Couch, G.S., Morris, J.H., and Ferrin, T.E. (2018). UCSF ChimeraX: Meeting modern challenges in visualization and analysis. Protein Sci. *27*, 14–25.

STAR★METHODS

KEY RESOURCES TABLE

REAGENT or RESOURCE	SOURCE	IDENTIFIER
Antibodies		
G2	Produced house[27]	N/A
CV-30	Produced in house[71]	N/A
4C2	Produced in house[24]	N/A
S41	Produced in house[70]	N/A
Goat Anti-Human IgG-HRP	SouthernBiotech	Cat# 2040-05; RRID:AB_2795644
Anti-mouse IgG, HRP-linked Antibody	Cell Signaling Technology	Cat# 7076S
HRP-Conjugated Streptavidin	Thermo Scientific	Cat# N100
I1-Hybridoma (Anti-VSV antibody)	ATCC	Cat# CRL2700
Bacterial and virus strains		
Mouse adapted MERS-CoV (m35c4) virus stock	Produced in house	N/A
Chemicals, peptides, and recombinant proteins		
MERS-CoV S2P	Produced in house[19]	N/A
MERS-CoV S2P I53-50A	Produced in house	N/A
MERS-CoV S2P T33_dn10A	Produced in house	N/A
MERS-CoV RBD I53-50A	Produced in house	N/A
MERS-CoV RBD	Produced in house	N/A
MERS-CoV NTD I53-50A	Produced in house	N/A
MERS-CoV NTD	Produced in house	N/A
Human DPP4-Fc (CD26)	Produced in house	N/A
Immobilized Papain	Thermo Scientific	Cat# 20341
Immobilized Protein G	Thermo Scientific	Cat# 20397
Ni Sepharose(TM) Excel	Cytiva	Cat# 17371202
AddaVax Adjuvant	InvivoGen	Cat# vac-adx-10
AVIDITY LLC BirA biotin-protein ligase bulk reaction kit	Fisher Scientific	Cat# NC9204985
SureBlue Reverve TMB 1-Component Microwell Peroxidase Substrate	SeraCare	Cat# 5120-0083
Gibco™ DMEM, high glucose	Fisher Scientific	Cat# 11-965-126
Cytiva HyClone Fetal Bovine Serum	Cytiva	Cat# SH30396.03
Penicillin-Streptomycin (10,000 U/mL)	Life Technologies	Cat# 15140163
Gibco™MEM, Hanks' Balanced Salts	ThermoFisher Scientific	Cat# 11575032
Lipofectamine 2000 Transfection Reagent	Life Technologies	Cat# 11-668-500
Deposited data		
Negative stain EM map of polyclonal serum from mouse immunized with MERS-CoV NTD-I53-50 in complex with MERS S-2P	EMDataBank	EMD-47577
Negative stain EM map of polyclonal serum from mouse immunized with MERS-CoV S-2P in complex with MERS S-2P	EMDataBank	EMD-47580
Negative stain EM map of polyclonal serum from mouse immunized with MERS-CoV S-2P in complex with MERS S-2P	EMDataBank	EMD-47583
Negative stain EM map of polyclonal serum from mouse immunized with MERS-CoV S-2P-I53-50 in complex with MERS S-2P	EMDataBank	EMD-47584

(*Continued on next page*)

Continued

REAGENT or RESOURCE	SOURCE	IDENTIFIER
Negative stain EM map of polyclonal serum from mouse immunized with MERS-CoV S-2P-I53-50 in complex with MERS S-2P	EMDataBank	EMD-47585
Negative stain EM map of polyclonal serum from mouse immunized with MERS-CoV S-2P-T33_dn10 in complex with MERS S-2P	EMDataBank	EMD-47586
Negative stain EM map of polyclonal serum from mouse immunized with MERS-CoV S-2P-T33_dn10 in complex with MERS S-2P	EMDataBank	EMD-47587
Negative stain EM map of polyclonal serum from mouse immunized with MERS-CoV RBD-I53-50 in complex with MERS S-2P	EMDataBank	EMD-47588
Negative stain EM map of polyclonal serum from mouse immunized with MERS-CoV RBD-I53-50 in complex with MERS S-2P	EMDataBank	EMD-47589
Negative stain EM map of polyclonal serum from mouse immunized with MERS-CoV RBD-I53-50 in complex with MERS S-2P	EMDataBank	EMD-47592
Experimental models: Cell lines		
Expi293F	ThermoFisher	Cat# A14527
Huh7	JCRB	Cat# JCRB0403
Vero81	ATCC	Cat# CCL-81
Experimental models: Organisms/strains		
BALB/c mice	Jackson Laboratory	Cat# 000651
288/330-hDPP4 transgenic mice	Produced in house[101]	N/A
Recombinant DNA		
See Table S1 for amino acid sequences	N/A	N/A
Software and algorithms		
PyMol	Schrodinger, LLC	https://pymol.org/2/
Prism 9	GraphPad	https://www.graphpad.com/scientific-software/prism/
Unicorn 7.0	GE Healthcare	http://www.gelifesciences.com/
CryoSparc	Punjani et al.[129]	https://cryosparc.com/
EPU	Thermo Fisher	https://www.thermofisher.com/us/en/home/electron-microscopy/products/software-em-3d-vis/epu-software.html
UCSF Chimera	Pettersen et al.[130]	https://www.cgl.ucsf.edu/chimera/
UCSF ChimeraX	Goddard et al.[131]	https://www.rbvi.ucsf.edu/chimerax/
Other		
Filter paper	Cytiva	Cat# 1004047
Uranyl Formate	SPI Chem	Cat# 02545-AA
Superdex 200 Increase SEC column	Cytiva	Cat# 28-9909-44
Superose 6 Increase SEC column	Cytiva	Cat# 29091596
MAX Efficiency™ DH5α Competent Cells	Sigma-Aldrich	Cat# I6758
EndoSafe LAL Test Cartridges	Charles River Labs	Cat# PTS20005F
Octet Protein A Biosensors	Sartorius	Cat# 18-5010
Plasmid Plus Maxi Kit	Qiagen	Cat# 12963
Kanamycin Sulfate	Sigma-Aldrich	Cat# K1876
96 Well Flat-Bottom Immuno Plate	Thermo Scientific	Cat# 442404

EXPERIMENTAL MODEL AND STUDY PARTICIPANT DETAILS

Cell lines

Expi293F cells are derived from the HEK293F cell line (Life Technologies). Cells were grown in Expi293 Expression Medium (Life Technologies), cultured at 36.5°C with 8% CO_2 and shaking at 150 rpm Huh7 cells cultured in DMEM with 10% FBS (Hyclone), 1% PenStrep (100 I.U./mL penicillin and 100 μg streptomycin) and cultured at 37°C with 5% CO_2. Vero81 cells were cultured in DMEM (Gibco: 11995065 + 5% FBS (VWR: 76237-678) + 1% Pen/Strep (Gibco; 15140122) at 37°C with 5% CO_2.

Mice

For immunogenicity studies, female BALB/cAnNHsd were purchased from Envigo (order code 047) at 7 weeks of age. Mice were housed in a specific-pathogen free facility within the Department of Comparative Medicine at the University of Washington, Seattle, accredited by the Association for Assessment and Accreditation of Laboratory Animal Care (AAALAC). Animal studies were conducted in accordance with the University of Washington's Institutional Animal Care and Use Committee.

For *in vivo* protection studies, 288/330-hDPP4 transgenic mice were used, which were bred and maintained at the University of North Carolina at Chapel Hill (Animal Welfare Assurance #A3410-01). The study was performed using protocols (#23–085) approved by the UNC Institutional Animal Care and Use Committee (IACUC) and carried out in accordance with the recommendations for care and use of animals by the Office of Laboratory Animal Welfare (OLAW), National Institutes of Health, and the IACUC. Immunizations were performed in a BSL2 facility accredited by the Association for Assessment and Accreditation of Laboratory Animal Care (AAALAC).

METHOD DETAILS

Protein purification and characterization

All constructs contained a C-terminal histidine affinity tag and were codon optimized by GenScript for mammalian cell expression. Expi293F cells were transiently transfected using PEI MAX and cultured for three days 37°C. Cells were harvested, centrifuged, and filtered to obtain clarified supernatants. Clarified cell supernatants were buffered with 5 mL of 5M NaCl and 7 mL of Tris pH 8.0 per 100 mL of supernatant and batch bound with Ni Sepharose Excel resin while shaking for 30 min to an hour at room temperature. Resin were collected in a gravity column, washed with five column volumes of wash buffer containing 25 mM Tris pH 8.0, 150 mM NaCl, and 30 mM imidazole, and eluted with three column volumes of elution buffer comprised of 25 mM Tris pH 8.0, 150 mM NaCl, and 300 mM imidazole. Eluted component constructs were further purified using SEC on either a Superose 6 Increase 10/300 gel filtration column if they were spike-bearing, or a Superdex 200 Increase 10/300 gel filtration column if they were domain-bearing constructs. *In vitro* assembly of nanoparticles was conducted using a 1:1 M ratio of each component and incubated at room temperature for 30 min with rocking. Following nanoparticle assembly, all particles were purified one last time through a Superose 6 Increase 10/300 column. All spike and NTD protein components and assembled nanoparticles were purified into 50 mM Tris pH 8.0, 150 mM NaCl, 0.25% w/v Histidine, and 5% glycerol. The RBD component and nanoparticle were purified in 50 mM Tris pH 7.4, 185 mM NaCl, 100 mM Arginine, 4.5% Glycerol, and 0.75% CHAPS.

Bio-layer interferometry (BLI)

All samples were diluted in kinetics buffer (0.05% bovine serum albumin and 0.01% Tween 20 in PBS) and measurements were carried out using an Octet Red 96 system at 25°C shaking at 1000 rpm. Antibodies were diluted to a final concentration of 20 μg/mL before being immobilized on ProteinA tips (Sartorius) for 600 s. Unassembled and nanoparticle proteins were diluted to 250 nM and associations were measured for 600 s, followed by dissociation for 900 s in kinetics buffer.

Nano differential scanning fluorimetry

The thermal stabilities of the MERS-CoV and SARS-CoV-2 S-2P trimers were measured at 0.40 mg/mL in the presence of the hydrophobic dye 20× SYPRO Orange using an UNcle (UNchained Labs). Changes in fluorescence emission were used to evaluate protein unfolding as readings were measured from 25°C to 95°C with an increasing ramp rate of 1 °C/min.

Aggregation temperature (T_{agg}) determination

Aggregation of nanoparticle immunogens at 0.20 mg/mL was evaluated using an UNcle (UNchained Labs). DLS was monitored from 25°C to 95°C with an increasing ramp rate of 0.15 °C/min and an acquisition time of 10 s to measure changes in particle size or aggregation state as a function of temperature.

Immunogenicity studies

For each immunization, low-endotoxin nanoparticles were diluted to 20 μg/mL in buffer and mixed with 1:1 v/v AddaVax adjuvant (InvivoGen vac-adx-10) to obtain a final dose of 1 μg of immunogen per animal per injection (Figures 2, S2, S3, and S5–S7). At 8 weeks of age, 10 mice per group were injected subcutaneously in the inguinal region with 100 μL of immunogen at weeks 0 and 4. Animals were bled using the submental route at weeks 0, 2, and 6. A terminal bleed was collected at week 8 via cardiac puncture. Whole blood

was collected in serum separator tubes (BD #365967) and rested for 30 min at room temperature for coagulation. Tubes were then centrifuged for 10 min at 2,000 *g* and serum was collected and stored at −80°C until use.

288/330-hDDP4 transgenic mouse vaccinations and virus challenge experiments

The subsequent challenge study was conducted in a BSL3 facility at the University of North Carolina. Briefly, groups of 288/330-hDPP4 transgenic mice (n = 5/6 per condition and time point, mixed sexes, ∼19–23 weeks of age) were vaccinated subcutaneously in the inguinal region with 100 μL of immunogen with 1 μg of nanoparticle immunogen at weeks 0 and 4 (Figures 4 and S8). Animals were bled via submandibular route at −1, 2, and 6 weeks. Mice were then moved into the BSL3 and acclimated for a few days. For infection, mice were anesthetized with an intraperitoneal delivery of xylazine and ketamine and intranasally inoculated with 1×10^5 PFU of MERS-CoV maM35c4. Mice were monitored daily for weight loss and mortality. On 3 dpi and 5 dpi, groups of mice were euthanized with isoflurane and nasal turbinates and the caudal lobe of the right lung were collected to determine viral load by plaque assay. For plaque assay, harvested tissues were homogenized in 1× PBS, and the resulting homogenate was serial-diluted onto a confluent monolayer of Vero E81 cells, followed by agarose overlay. Plaques were then visualized with an overlay of Neutral Red on 3 dpi.

Enzyme-linked immunosorbent assay (ELISA)

Costar 96-well high protein binding plates were coated overnight at 4°C with spike proteins at 2 μg/mL and blocked in 200 μL of blocking buffer composed of (TBST: 1x Tris-buffered saline with 25 mM Tris pH 8.0, 150 mM NaCl, 0.2% Tween 20, and 5% nonfat milk). Plates were then washed 3x with TBST in an automated plate washer (Biotek); all washing steps follow the same protocol. 3-fold serial serum dilutions were made starting at 1:100 and 100 μL were plated and incubated for 1 h at room temperature shaking at 500 rpm. Plates were washed then 100 μL of secondary anti-mouse (Cell Signaling Technology) (1:2,000 dilution) or anti-human (SouthernBiotech) (1:5,000 dilution) IgG-HRP were added to each well and incubated shaking at room temperature. Plates were washed before 100 μL per well of TMB were added and developed for 3 min, then quenched with 100 μL of 1N HCl. Reading at absorbance at 450 nM was carried out with an Epoch plate reader (Biotek).

Competition ELISA

Competition ELISAs were performed in a similar manner as the aforementioned ELISA method with minor adjustments. To determine fixed competitor concentrations for 80% maximal binding against S-2P, a 3-fold serial dilution series with a starting dilution of 1:10 was carried out in blocking buffer and 100 μL per well of were applied and incubated on plates coated with S-2P for 45 min then washed. 100 μL per well of Goat anti-human IgG-HRP secondary (1:20,000 dilution) was plated for 30 min at room temperature. Plates were washed then developed for 2 min with 100 μL of TMB and quenched with 100 μL of 1 N HCl. The concentration of competitors at which approximately 80% of maximal binding observed was used for competition assays.

As a positive control for achieving full competition against the competitor, hDPP4-Fc and G2 were biotinylated using EZ-Link Sulfo-NHS-LC-Biotin (Thermo Scientific) and 80% maximum binding concentrations against S-2P were determined with biotinylated proteins (hDPP4-Fc-biot and G2-biot). For hDPP4-Fc self-competition, a 3-fold serial dilution was performed starting at 300 μg/mL of hDPP4-Fc in blocking buffer and 100 μL per well was plated on S-2P coated plates for 30 min. Plates were washed and 100 μL per well of biotinylated hDPP4-Fc at 8 μg/mL was added and incubated for 45 min. Plates were washed and 100 μL per well of secondary HRP-conjugated Streptavidin (1:5,000 dilution) (Thermo Scientific) was plated for 30 min. Plates were washed one last time then developed for 2 min with TMB and quenched with 1 N HCl before reading. For G2 self-competition, a 3-fold serial dilution of G2 starting at 25 μg/mL was carried out and added to S-2P coated plates for 30 min and washed before biotinylated G2 was added as the competitor at 0.37 μg/mL for 45 min then washed. 100 μL of secondary HRP-Conjugated Streptavidin was added for 30 min before plates were washed and developed with TMB for 2 min before being quenched with 1 N HCl.

For the serum competition assay, 3-fold serial serum dilutions were performed starting at 1:10 in blocking buffer, transferred to S-2P-coated plates and incubated at room temperature for 30 min, then washed. 100 μL per well of hDPP4-Fc or G2 at 1.11 μg/mL or 0.12 μg/mL, respectively, was added and incubated for 45 min then washed. Goat anti-human IgG-HRP at a 1:20,000 dilution was added for 30 min. Plates were developed for 2 min and optical densities were read at 450 nm.

Generation of pseudoviruses

To produce pseudoviruses for entry and neutralization assays, HEK293T cells were seeded in Dulbecco's Modified Eagle Medium (DMEM) enriched with 10% Fetal bovine serum (FBS, Hyclone), 1% PenStrep (100 I.U./mL penicillin and 100 μg streptomycin) (Gibco 15140-122) at the appropriate density to yield 80% confluency in polylysine-coated 100 mm cell culture dishes and placed in an incubator at 37°C with 5% CO_2. After 18–22 h incubation, cells were washed with OPTI-Minimum Essential Media (Opti-MEM, Life Technologies). 24 μg of MERS-CoV-EMC, MERS-CoV-London, MERS-CoV-South Korea, MERS-CoV-Kenya full length S plasmids were prepared in 1.5mL of OPTI-MEM and combined with 60μL of Lipofectamine 2000 (Life Technologies) diluted in 1.5mL of OPTI-MEM and incubated at room temperature for 15–20 min. The mixture was added to the HEK293T cells which were placed for 2 h in an incubator at 37°C with 5% CO_2 after which 2mL of DMEM enriched with 20% FBS and 2% PenStrep (200 I.U./mL penicillin and 200 μg streptomycin) was added to the transfected cells and incubated overnight. The following day, cells were washed with DMEM and transduced with VSVΔG/Fluc and incubated for 2 h at 37°C with 5% CO_2. After washing with DMEM, medium

supplemented with anti-VSV-G antibody (I1-mouse hybridoma supernatant diluted to 1:25 from CRL-2700, ATCC) was added to the cells to reduce background from the parental virus and an additional incubation at 37°C with 5% CO_2 was performed overnight. The next day, the supernatant from the cells was harvested from the 100 mm dishes, further clarified by centrifugation at 3,000xg for 10 min, filtered (0.45μm), and concentrated 10 times by using centrifugal devices with 30 kDa cutoff membranes. Pseudoviruses were then aliquoted and frozen at −80°C until used.

Pseudovirus neutralization assay

Huh7 cells cultured in DMEM with 10% FBS (Hyclone), 1% PenStrep (100 I.U./mL penicillin and 100 μg streptomycin) were subsequently trypsinized, counted and reseeded at ~30,000 cells per well in cell-culture grade 96 well plates and placed in an incubator at 37°C with 5% CO_2 overnight. The next day, after cell health and confluency was evaluated, a half-area 96-well plate was prepared with a 1:3 serial dilution of sera in DMEM in 22 μL final volume. 22 μL of pseudovirus was then added to each well and incubated at room temperature for 30–45 min. The media was removed from Huh7 cells and they were subsequently washed 2-3x and 40 μL of the sera/pseudovirus mixture from the half area plate was added to the cells and incubated for 2 h at 37°C with 5% CO_2 before adding 40 μL of 20% FBS and 2% PenStrep (200 I.U./mL penicillin and 200 μg streptomycin) containing DMEM. Following 18–22 h incubation, 40 μL of One-GloEX (Promega) was added to the cells and incubated in the dark for 5 min prior to reading on an Agilent BioTek *Neo*2 plate reader. Relative luciferase units were plotted and normalized in Prism (GraphPad) using a zero value of cells alone and a 100% value of 1:2 virus alone. Nonlinear regression of log(inhibitor) vs. normalized response was used to determine ID_{50} values from curve fits. At least two biological replicates with two distinct batches of pseudovirus were conducted for each serum sample.

Negative stain electron microscopy (nsEM)

400-mesh carbon coated grids (Electron Microscopy Sciences) were glow-discharged and 3 μL of 20 μg/mL nanoparticles were applied then stained with 2% (w/v) uranyl formate. All nsEM data were collected with a BM-Ceta camera at 57,000x magnification using EPU 2.0 on a 120 kV Talos L120C transmission electron microscope (Thermo Scientific). CTF processing, particle picking, particle extraction, 2D classification, and 3D refinement steps were all performed with CryoSPARC.[135]

Ns-EMPEM

To obtain Fabs for immune complexes, 500 μL of serum from mice were pooled from the terminal bleed time point to maximize the workable volume for processing. Sera were incubated with Pierce Protein G Agarose (Thermo Fisher) at pH 5.0 for 12–24 h at 4°C and polyclonal antibodies were washed with five column volumes of PBS to remove unbound sera and eluted from gravity filtration columns with three column volumes of 0.1 M glycine, pH 2.5 and neutralized with 1 M Tris pH 8.0 to a final diluted concentration of 50 mM Tris pH 8.0. Eluted IgGs were cleaved with papain in 20 mM NaPO4, pH 6.5, 10 mM EDTA, 20 mM Cysteine at 37°C with shaking for 5–20 h. Cleaved Fabs were retrieved using gravity filtration columns and dialyzed into PBS before the final step of SEC in a Superdex 200 Increase 10/300 gel filtration column equilibrated with PBS. To prepare immune complexes for ns-EMPEM, purified Fab and MERS S-2P were mixed at a 5:1 ratio and incubated at room temperature with rocking for 30–45 min, then immediately applied onto glow-discharged 400-mesh carbon coated grids for ns-EMPEM. Three rounds of 2D classification were performed, selecting for only spike proteins with clear bound Fab densities. Ab initio 3D reconstruction followed by heterogeneous refinement with no symmetry was used to generate 3D models of immune complexes. Only classes with distinct spike densities that captured a representation of bound Fabs were further processed with 3D refinement. Chimera[136] and ChimeraX[137] were used to make figures.

QUANTIFICATION AND STATISTICAL ANALYSIS

Group comparisons were conducted using one-way ANOVA with Geisser-Greenhouse correction followed by Dunnett's multiple comparison in Prism 9 (GraphPad). Differences were considered significant when p values were less than 0.1. Data were also analyzed with two-way ANOVA or mixed model followed by Sidak's multiple comparison. Differences were considered statistically significant when p values were less than 0.05.